J. Fluid Mech. (1986), *vol.* 163, *pp.* 283–322
Printed in Great Britain

An experimental investigation of a turbulent shear flow with separation, reverse flow, and reattachment

By R. RUDERICH AND H. H. FERNHOLZ
Hermann-Föttinger-Institut, Technische Universität, Berlin

(Received 31 January 1985 and in revised form 9 September 1985)

Experiments were performed in the highly turbulent and disturbed flow over a bluff plate with a long splitter plate in its plane of symmetry. The flow separates at the sharp bevelled edge of the bluff plate, forms a free shear layer on top of the reverse-flow region which is bounded on its other side by the splitter plate, and reattaches on the splitter plate over a narrow region curved in spanwise direction. Downstream of reattachment the shear flow adjusts slowly to the wall boundary conditions.

Measurements of mean velocity, Reynolds-shear-stress and Reynolds-normal-stress distributions were carried out by hot-wire and pulsed-wire anemometry. The latter technique was used in those regions of the flow where reverse flow occurred or where the flow was highly turbulent. Spectra and integral lengthscales were measured to investigate the state and structure of the flow. The large-eddy structure in the inner region of the flow had lengthscales in the two cross-stream directions which were approximately equal, indicating a fast break-up of spanwise structures just downstream from separation.

Mean and fluctuating quantities showed a self-similar behaviour in a short region upstream of reattachment and 'profile similarity' in the separated shear layer and along the splitter plate downstream from reattachment. Probability-density distributions of skin friction were measured and used to calculate mean and fluctuating values. No flapping of the reattaching shear layer could be observed. Pulsed-wire measurements revealed that the logarithmic law of the wall does not hold either in the reverse-flow region or in a region about half the length of the bubble downstream from reattachment.

1. Introduction

Turbulent shear flows containing regions with high levels of turbulence ($T_u > 30\,\%$), instantaneous or mean reverse flow, separation and reattachment occur in many technical applications. They may be generated by numerous geometrical configurations (e.g. Kottke 1983), some of which are shown in figure 1. The first two model flows, the backward-facing step (*a*) and the blunt plate (*b*), have been investigated in considerable detail, and references may be found in Eaton & Johnston (1981), Kiya & Sasaki (1983) and Cherry, Hillier & Latour (1984). Configurations (*c*)–(*e*) are of the blunt-forebody/splitter-plate type, where the splitter plate is so long that no interaction occurs between the upper- and lower-side shear layer. In case (*c*) – the flow investigated in this paper – a thin laminar boundary layer on the bluff plate separates at the sharp bevelled edge, forms a curved mixing layer – bounded on its lower side by a reverse-flow region – and reattaches on to the splitter plate. This is a simplified

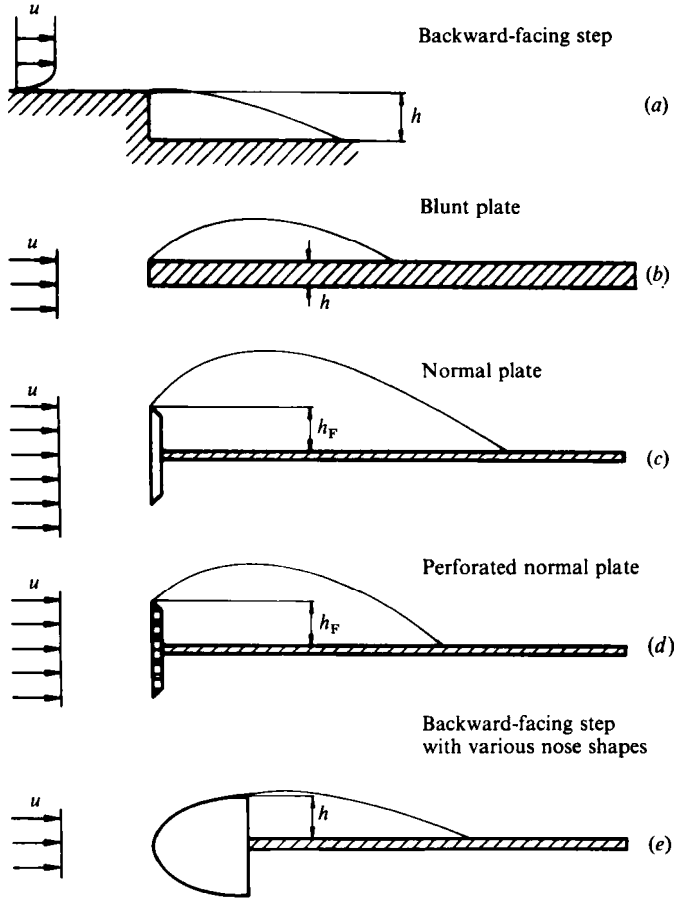

FIGURE 1. Flow configurations with separation and reattachment.

description of the flow, since it does not take into account a reseparation line about two fence heights downstream from the bluff plate on the splitter plate (cf. figure 4*a*), a curved reattachment region due to three-dimensional effects near the tunnel sidewalls, and an attached shear layer readjusting much slower than expected (see also Bradshaw & Wong 1972) to the state of a nominally zero-pressure-gradient equilibrium turbulent boundary layer. This readjustment process is accompanied by large changes in the size and distribution of Reynolds normal and Reynolds shear stresses as well as in the size of the coherent structures of the flow.

Our choice of the bluff-plate/splitter-plate configuration (*c*) was influenced by the following considerations: the influence of an upstream boundary layer should be negligible, separation should be fixed, and the reverse-flow region should extend far enough into the flow so that aerodynamic interference effects of available probes would be as small as possible. This latter condition determined the height of the bluff plate which fixed the aspect ratio of the configuration, the blockage ratio and the length of the reverse-flow region.

De Brederode (1975) investigated the effects of side plates and aspect ratio on the two-dimensionality of the flow of configurations (*a*) and (*b*) and of a forward-facing step. He found that the flow was nominally two-dimensional if the aspect ratio was larger than 10, with the aspect ratio formed by tunnel width or side-plate distance and height of the step or thickness of the plate. Although not obvious at first sight, these considerations cannot be transferred to the present flow configuration, where it was impossible to obtain two-dimensional flow, even for aspect ratios larger than 10. Here two questions arise: (*a*) What are the appropriate lengthscales to define the aspect ratio? and (*b*) Is the three-dimensional behaviour – represented, for example, by the corner vortices and the curved reattachment line – specific to configuration (*c*)?

In the present flow configuration one may define the step height as the total height D of the bluff plate or the height h_F of the fence above the splitter plate which, for a symmetric configuration, is $0.5(D-t)$, where t is the thickness of the splitter plate. Using these two plate heights leads one to aspect ratios of 10 and 22, respectively. Nevertheless, strong effects of three-dimensional flow were observed downstream of the bluff plate, and de Brederode's minimum aspect ratio may be too small for such an 'overwhelmingly disturbed flow'. The ratio of tunnel width w to the length of L_R of the reverse-flow region may be a better criterion ($w/L_R = 1.54$ in the present T-shaped configuration), but a verification needs experiments in a larger wind tunnel, which are under way.

For a comparison with the flow downstream of a backward-facing step and a blunt plate (configurations (*a*) and (*b*)) oil-flow visualization was performed on the surface. In both cases the reattachment line was parallel to the separation edge and only a small corner vortex appeared downstream of the step. In the case of the backward-facing step the ratio w/L_R was 7 and the oncoming boundary layer turbulent. So the curved reattachment line appears to be specific to the T-shaped configuration.

Side plates were also used in the hope of improving the two-dimensionality of the flow. As is shown in figure 4(*b*), the number of corner vortices doubled and the three-dimensionality of the flow in the reverse-flow region increased. These findings excluded the use of the side plates for this experiment.

Plate heights D of 28 and 50 mm were used – the former for the measurement of wall data only – which led to blockage ratios of 5.7 and 10%, respectively. Thus blockage effects cannot be neglected in this experiment. They have been investigated for the present flow configuration by Smits (1982), and our own measurements confirm Smits' results by showing a decrease in reattachment length and an increase in bubble height with blockage. Attention should be drawn also to the influence of the turbulence level of the oncoming flow on the mixing layer and on the length of the reverse-flow region. Kiya & Sasaki (1983) found that L_R was reduced by 5% if the free-stream turbulence level was increased from 0.2 to 0.4%.

The general properties of the flow field were not changed significantly by the larger of the two fences, and so a higher blockage ratio was traded against a 'high' reverse-flow region and a shorter reattachment region. It appears that small blockage effects and a higher degree of unsteadiness may go together, e.g. Cherry *et al.* (1984) and Kiya & Sasaki (1983). In these two 'blunt-plate' experiments humps were observed in velocity and wall-pressure spectra which could not be detected in the present experiment (cf. §6).

Table 1 presents a survey of characteristic parameters of the flow around a bluff-plate/splitter-plate configuration and shows clearly that there are few flow-field measurements and even less skin-friction data. This results largely from the lack of adequate measuring techniques, since hot-wire anemometry and conventional skin-

Author	Configuration	U_∞/ν (m^{-1})	c_{pm}	Tu_∞ (%)	Blockage ratio (%)	W/h_F	W/x_R	Drag	Static pressure	Skin friction	Mean velocity	Fluctuating velocity and pressure	Correlations, spectra	Miscellaneous
Arie & Rouse (1956)	⊢——— $\alpha = 90°$	8×10^4	n.m.	1.5	17	12	1.4	yes	n.m.	n.m.	yes	u', v', w' hot wire	n.m.	
Roshko & Lau (1965)	⊢——— $\alpha = 90°$	5.9×10^5	0.36 n.m.	0.03	2.5 5	213 58	6.3 2.4	n.m.	yes	n.m.	n.m.	n.m.	n.m.	Reattachment at various Reynolds numbers
Ranga Raju & Garde (1970)	⊢— >—— $\alpha = 90°, 135°$	8.3×10^5	n.m.	n.m.	16 12	6.3 8.1	n.m. n.m.	yes	n.m.	n.m. n.m.	n.m. n.m.	n.m. n.m.	n.m.	
Smits (1980, 1982)	⊢— <— $30° < \alpha < 90°$	2.3×10^5 to 1.1×10^7	0.40	n.m.	1 to 12	16 to 197	1.2 to 6.7	n.m.	yes	Preston tube	Pitot tube	n.m.	n.m.	Reattachment from extrapolation of τ_w
Hillier, Latour & Cherry (1983)	⊢——— $\alpha = 90°$	1.5×10^6	0.39	< 0.1	2.5	101	4.2	n.m.	yes	n.m.	n.m.	p'	p'-spectra	Reattachment from oil flow
Ruderich & Fernholz (1983)	⊢——— $\alpha = 90°$	6.4×10^5	0.39 0.41	0.66 0.66	5.7 10	45 22	2.0 1.3	n.m.	yes	Wall-pulsed wire	Hot wire and pulsed wire	h.w.: u' p.w.: u' w.p.w.: τ'	n.m.	Reattachment from oil flow and w.p.w. τ_w measurement

n.m. = not measured

TABLE 1. Characteristic parameters of the flow around a bluff-plate/splitter-plate configuration

friction devices fail in regions of high turbulence intensity or flow reversal. The only remaining measuring techniques for such flows are laser-Doppler (e.g. Stevenson, Thompson & Craig 1984) and pulsed-wire anemometry (Bradbury & Castro 1971; Castro & Dianat 1983). This latter technique has two advantages: (1) its costs are within the range of hot-wire anemometry; and (2) expertise obtained in developing hot-wire probes with low aerodynamic interference can be used.

The purpose of this paper is to fill this gap in the data for flow configuration (*c*) of figure 1 by using pulsed-wire anemometry in order to gain a better insight into the properties of the reverse-flow region, the development of the separated shear layer and the adjustment of the shear flow to the wall boundary conditions. It is also expected that the measured data will serve as starting conditions for calculation methods and for comparisons with their results.

Section 2 describes the experimental arrangement and the flow regime, illustrated by surface-oil-flow pictures and by smoke-visualization photographs in several planes of the flow. Measuring techniques, with emphasis on pulsed-wire anemometry, are discussed in §3. This is followed by a presentation of wall data and a discussion of three-dimensional effects (§§4 and 5). Finally, §6 presents mean and fluctuating data measured in the flow field, describing the development of the shear layer and its coherent structures as well as the redistribution of Reynolds shear and normal stresses downstream of reattachment. This section also covers the similarity behaviour of mean- and fluctuating-flow quantities and departures from the logarithmic law of the wall.

2. Experimental arrangement and flow regime

2.1. *Description of the test section and the wind tunnel*

The wind tunnel used in this investigation is described by Fernholz, Graham & Vagt (1982) and was operated in the steady mode. It is an open-circuit, suck-down tunnel with a centrifugal blower driven by a 13 kW motor at the downstream end. The motor was supplied from a variable output thyristor rectifier allowing a speed range from zero to 20 m s^{-1}. The tunnel inlet was fitted with a bellmouth followed by a honeycomb and two screens. The cross-section of the tunnel was 0.49×0.50 m, and the tunnel was constructed in sections which could be interchanged and removed so that various different tunnel combinations of 6 m maximum length were possible. One of these sections was the working section (1.55 m in length), fitted with a traverse gear, a glass window and the bluff-plate/splitter-plate configuration located on the centreline in a horizontal position. The bluff plate (fence) was steel with a smoothly polished surface 6 mm thick, with the edge machined to a sharp 30° bevel. The fence height h_F above the splitter plate (6.3 mm thick and 1.50 m long) was 11 and 22 mm respectively. The configuration spanned the tunnel width.

Symmetry of the flow on both sides of the splitter plate, obtained by careful adjustment and by means of three flaps at the downstream end, was confirmed by measurements of vertical pressure distributions at several spanwise positions in front of the bluff plate and by the oilflow pictures in figure 5.

The removable ceiling of the working section was of wooden blocks made airtight by rubber seals which fitted into grooves on both sides of the blocks. The traverse gear provided precise linear (incremental resolution 0.005 mm) and angular (resolution 0.1°) movements. For flow-visualization studies the wooden ceiling could be replaced by a window pane.

The flow field in the empty tunnel was optimized for steady-flow conditions and

uniform mean ($\pm 1\,\%$ maximum deviation from the mean velocity on the centreline), and fluctuating velocity profiles were obtained. The turbulence level across the tunnel was constant, apart from the top and bottom wall boundary layer, with $T_u = 0.66\,\%$ over the frequency range d.c. to 10^4 Hz.

The majority of tests were performed with the 22 mm fence at a Reynolds number $(u_\infty h_F/\nu) = 1.4 \times 10^4$, which results in a free-stream velocity of approximately 9.6 m s^{-1} measured at 17 total bluff-plate heights upstream. The laboratory was air-conditioned (room temperature held constant at 22.5 ± 0.3 °C) in order to minimize the drift of hot-wire and transducer calibrations.

2.2. *Flow regime and flow visualization*

An extensive preliminary investigation of the flow field has shown that important information can be obtained from flow-visualization studies both on the walls and in the flow field itself. A video film and still photographs were made, and a few of the latter are discussed below. Smoke-flow visualization was achieved by injecting kerosene smoke from a smoke generator through a slot along the stagnation line of the bluff plate. The smoke was illuminated by a 4.5 mm thick rotating 3 W laser beam (Mensing & Fiedler 1980). This technique permitted the positioning of light sheets in the (x, y)-, (x, z)- or (z, y)-plane as appropriate for the inspection of the flow (cf. figure 6 for the coordinate system).

For the flow photographs the free-stream velocity was varied between 1 and 14 m s^{-1}, giving Reynolds numbers of 1.5×10^3 and 2.1×10^5. Figure 2 shows three photographs of the flow (from left to right) in the (x, y)-plane along the centreline. The scale in flow direction is about 14 fence heights. At the lower Reynolds numbers single large coherent structures are visible, and figure 2(*b*) shows the roll-up of the separated shear layer into spanwise vortices and the pairing process. Figure 3, which presents the same flow situation from above (x, z-plane), reveals that the spanwise vortices are connected by longitudinal flow structures, as observed in plane mixing layers. None of these structures are visible further downstream, however. At the higher Reynolds number (figure 2*c*) the turbulence structure in the mixing layer is finer, and transition of the separated shear layer occurs very close to the bevelled edge.

The subsequent discussion refers to flow conditions at a Reynolds number $Re_{h_F} = 1.4 \times 10^4$, where the flow structure does not show any apparent further change with Reynolds number. Figure 4(*a*) presents the oil-flow pattern on the splitter plate (flow from left to right), revealing a spanwise, almost straight, limiting streamline 2.3 fence heights downstream of the bluff plate, a reverse-flow region, and a curved reattachment region. The limiting streamlines converge slightly towards the centreline in the reverse-flow region, an effect caused by the interaction of the flow on the tunnel sidewalls with the separated shear layer (cf. figure 5).

The limiting streamline ($F_S - S_S - F_S$) separates the near-wall fluid from the downstream side of the bluff plate and that from reattachment. It connects a saddle point (separation at $x/h_F = 2.3$) on the centreline with two foci located at about the same x-position but at $z = \pm 9.1 h_F$. The corner vortex on each side has already been observed by de Brederode & Bradshaw (1972) downstream of a step. The velocity – and thus the rotation – in the vortex is very small, as observed from the particle motion near the wall. The sense of rotation is such that the flow is directed downstream on the side of the vortex where it faces the tunnel sidewall.

Reattachment occurs at $x/h_F = 17.2 \pm 0.5$ on the centreline and at approximately $x/h_F = 15$ near the sidewall. Since the oil-flow picture represents only the 'mean footprint' of the flow, the width of the reattachment region could be indicative of

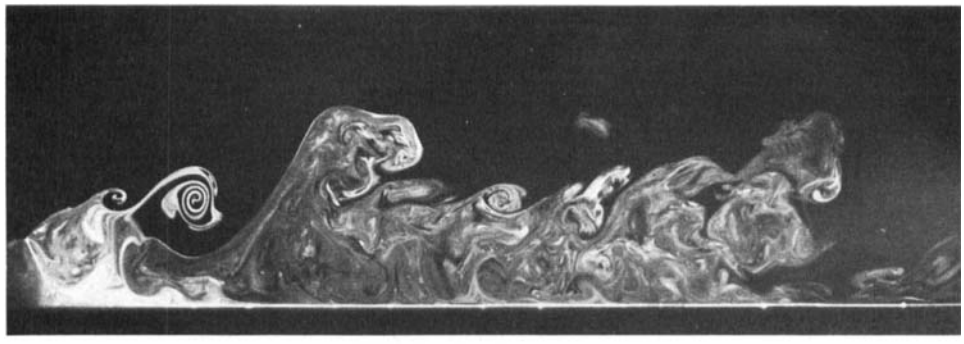

(*a*)

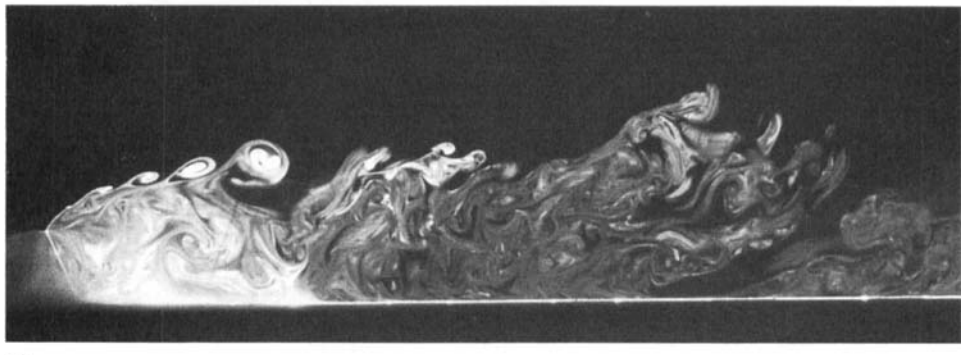

(*b*)

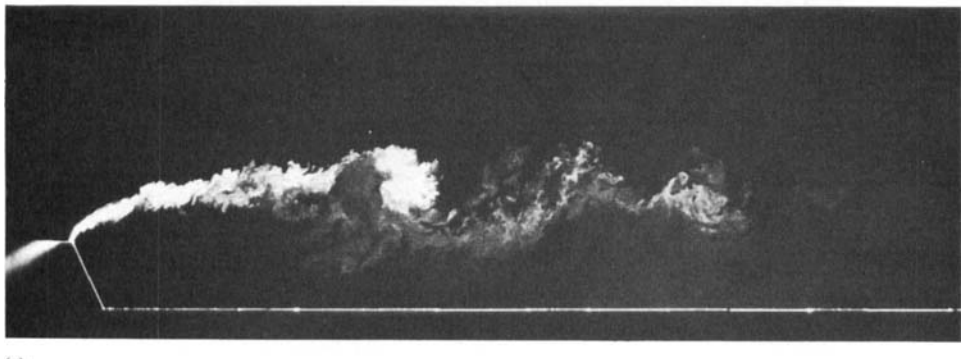

(*c*)

FIGURE 2. Smoke photographs of a separated shear layer in the (x, y)-plane at various Reynolds numbers: (*a*) $Re_{h_F} = 1.5 \times 10^3$; (*b*) 2.2×10^3; (*c*) 2.1×10^4.

the attachment of larger turbulence structures at the wall or of the flapping motion of the separated shear layer as a whole. A clear distinction between the two effects is not possible, although measurements of the u'-spectra showed neither a single peak nor a series of peaks.

Figure 5 shows the oil flow above and below the splitter plate on the tunnel sidewall, presenting further proof for the symmetry of the flow. The oil-flow pictures on the splitter plate and the tunnel sidewall are explained in a topological map in figure 6

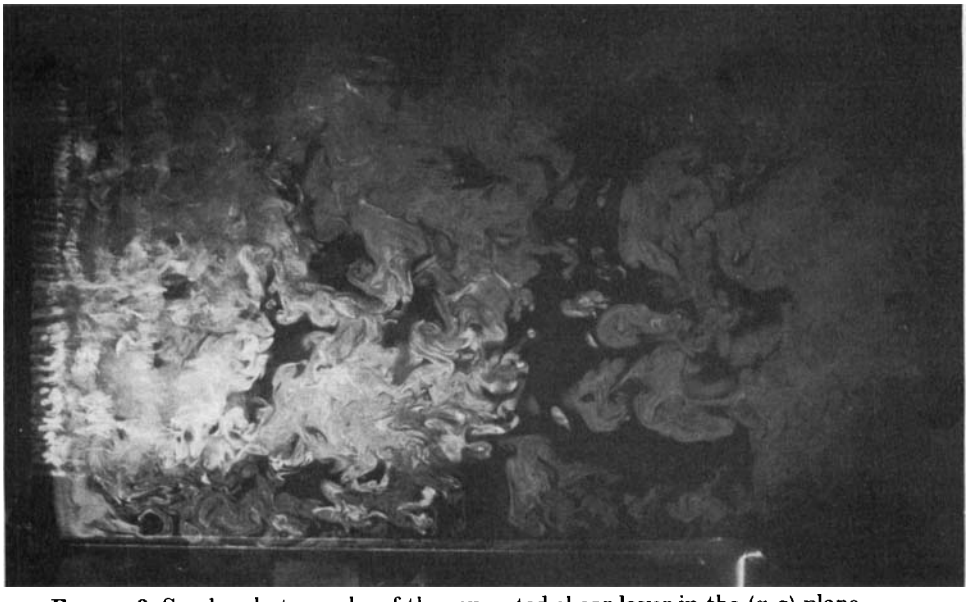

FIGURE 3. Smoke photographs of the separated shear layer in the (x, z)-plane 32 mm above the splitter plate ($Re_{h_F} = 1.5 \times 10^3$).

(*a*)

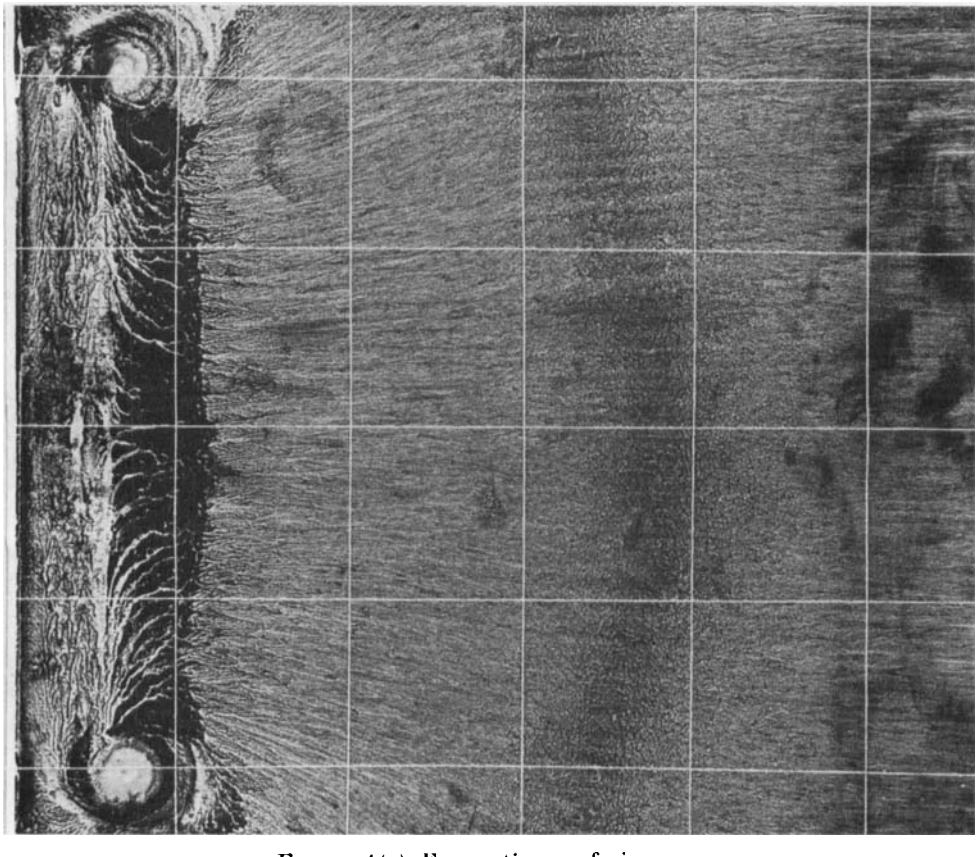

FIGURE 4(*a*). For caption see facing page.

which is *one* possible configuration, here confirmed by the flow visualization. The juxtaposition of a 'half' saddle on the sidewall and a 'half' node on the splitter plate, on the reattachment line intersection with the sidewall, follows from the directional pattern of the skin-friction field in the vicinity of the singular points. The numbers of critical points are consistent with the kinematic constraints, if all planes are taken into account.

(*b*)

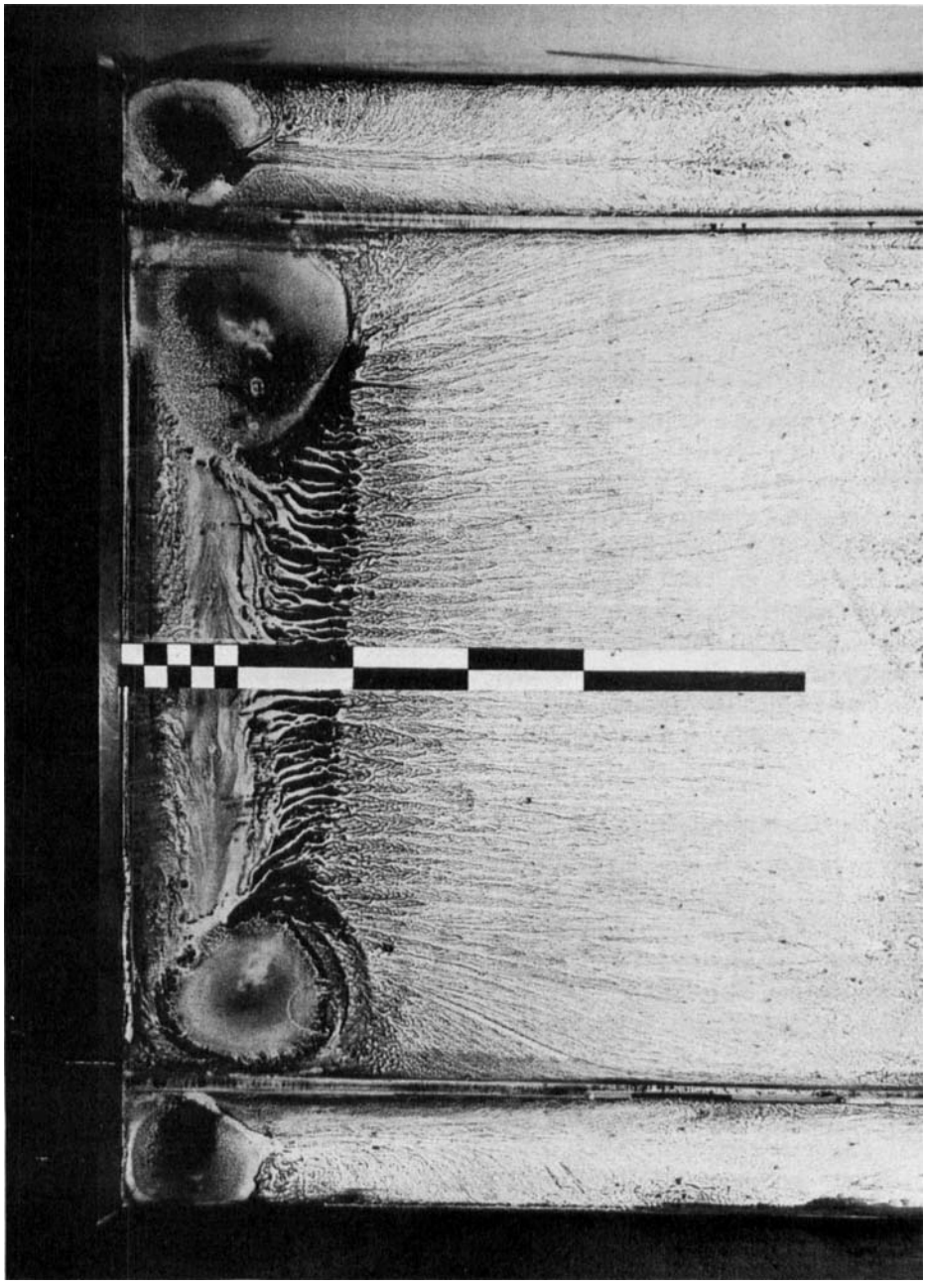

FIGURE 4. Oil-flow picture on the splitter plate ($Re_{h_F} = 1.4 \times 10^4$)
(*a*) without side plates; (*b*) with side plates.

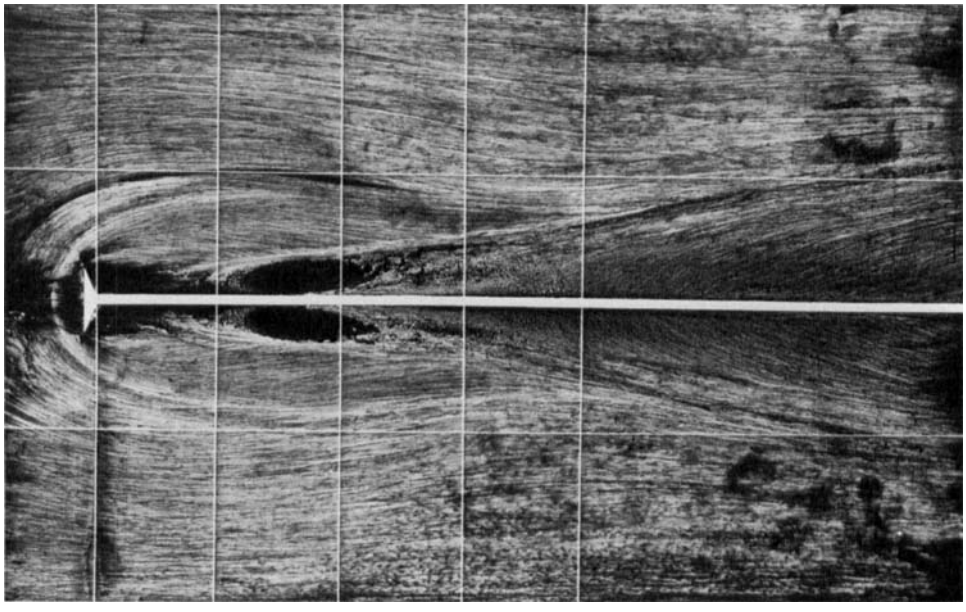

FIGURE 5. Oil-flow picture on the tunnel sidewall ($Re_{h_F} = 1.4 \times 10^4$).

At the intersection of the bluff plate with the tunnel sidewalls the wall boundary layer generates a system of four horseshoe vortices. Immediately downstream of the bluff plate the flow on the sidewall is in the downstream direction over the full height of the normal plate until it meets with a saddle point of separation. Downstream thereof the elliptically shaped mean footprint of the reverse-flow region on the sidwall is observed. The interacting sidewall/reverse-flow flow system transports fluid from downstream, along the corner and then in a downstream direction parallel to a line inclined at about 10° against the (x, z)-plane. The same flow system causes the reattachment region on the splitter plate to curve in an upstream direction.

3. Measuring techniques

Measurements of mean and fluctuating velocities were performed with Hermann-Föttinger-Institut (HFI)-made normal hot-wire probes (Dahm & Vagt 1977), X-wire probes, and normal-size and miniaturized pulsed-wire probes. The hot-wire probes and their error estimates are described by Fernholz & Vagt (1981) and the pulsed-wire probe by Dengel, Fernholz & Vagt (1982). All probes were mounted on the traverse gear described above and introduced into the flow through a slot in the roof of the test section.

Hot-wire measurements were carried out using a Prosser Scientific Instruments PSI 6110 anemometer which could be fitted for both analog and digital operation. Pulsed-wire measurements were performed by means of a modified PELA Flow Instruments anemometer (Bradbury & Castro 1971) interfaced to a CBM 3032 microcomputer so that on-line calibrations and measurements could be made using both PELA and our own software. Sample numbers ranged from 5000 for the flow field downstream from reattachment to 10000 for the reverse-flow region. Higher moments (skewness and flatness) were calculated for some velocity distributions and for all skin-friction data.

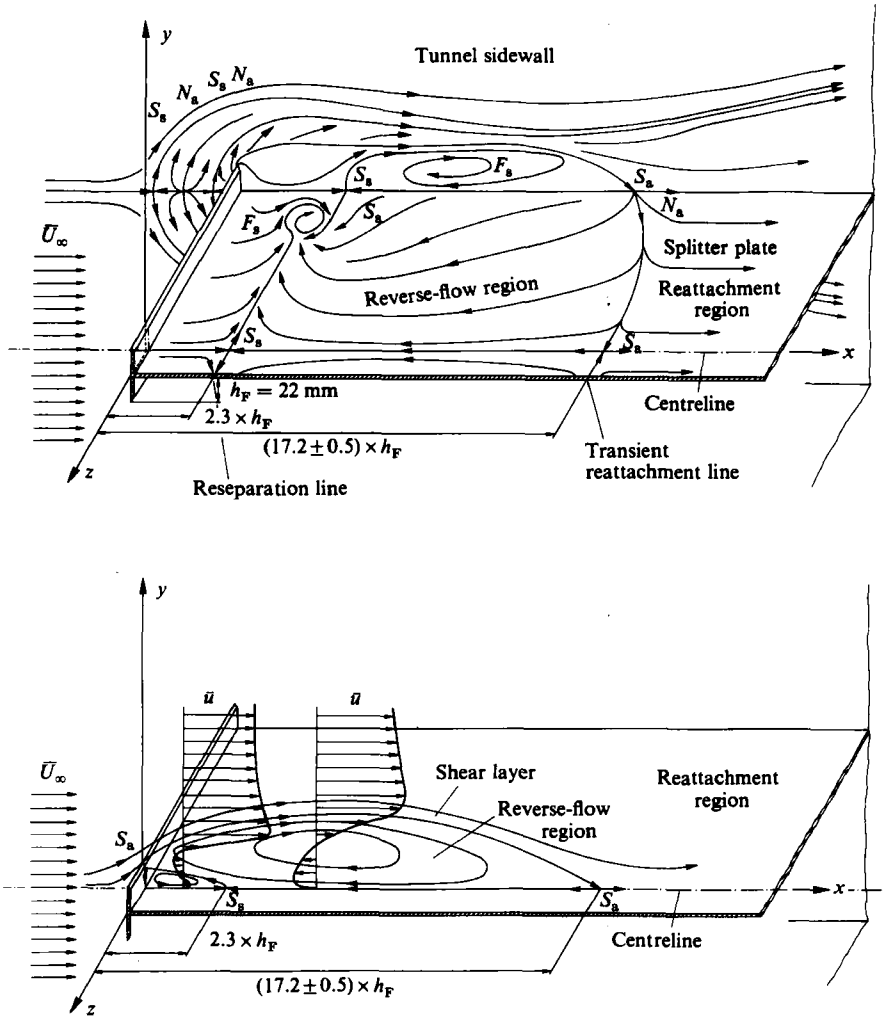

FIGURE 6. Schematic diagram of the mean flow downstream of a normal plate with a long splitter plate ($Re_{h_F} = 1.4 \times 10^4$).

Hot wires and pulsed wires were calibrated in the free stream of the test section without the bluff plate in position. The turbulence level was 0.66% and the mean velocity distribution uniform in the range $20 < y < 180$ mm normal to the splitter plate. An automatic micromanometer with a resolution of 0.005 mm water column was used to evaluate the flow speed measured by means of a Prandtl tube with 3 mm outer diameter.

The hot-wire and pulsed-wire calibrations were checked after each profile measurement and, if the wires or the calibration were found to be suspect, the measurements were discarded. The larger pulsed-wire probes were rather sensitive to dust deposits and had to be cleaned throughly after approximately five hours of running.

Integration time for the hot-wire data was 50 s, which is about five times as much as in an equilibrium low-turbulence boundary layer. This is indicative of the rather large turbulence structures due to the separated shear layer (see the discussion of the integral lengthscales in §§5 and 6).

Aerodynamic interference between the flow in the reverse-flow region and the probes was checked by measurements of a hot-wire probe, the prongs of which emerged through the splitter plate (e.g. Rogers & Head 1969). Comparisons between the signals of the two probes gave very good agreement in the vicinity of the wall, so that disturbances of the flow due to the probe (with a stem diameter of 3 mm) intruding through the mixing layer may be assumed to be negligible.

For the skin-friction measurements several techniques were tested since it was unknown *a priori* where the logarithmic law of the wall would hold and how severely instantaneous reverse flow would influence the measurements. The wall pulsed wire finally turned out to be the instrument (Ginder & Bradbury 1973; Eaton & Johnston 1980) which was best suited for this experiment and probably superior to the surface fence.

The probe as described by Castro & Dianat (1983) consists essentially of three fine parallel tungsten wires about 2 mm long and about 50 μm above the surface of a circular plug carrying the wire supports. This plug is mounted flush with the splitter plate. The central wire is rapidly heated by a short (5 μs) electrical pulse, and the time taken for the heat pulse to travel to the downstream or upstream wire is measured by operating the sensor wires in a constant-current differential bridge and is a measure of the instantaneous wall shear stress. The electronics required are identical with those used by the standard pulsed-wire anemometer, and the probe was interfaced to a CBM 3032 microcomputer allowing on-line calibration and measurement of surface stress. The instrument was calibrated directly in terms of surface shear stress $\bar{\tau}_w$ against a Preston tube in a zero-presure-gradient turbulent boundary layer using the calibration of Patel (1965). The only assumption which had to be made for the calibration was that the instantaneous velocity profile between the wall and the position of the wire is linear. This was checked by preliminary correlation measurements between two hot wires in the immediate vicinity of the wall.

The wall pulsed wire permits measurements of mean and fluctuating values of skin friction. For the calibration the function

$$\bar{\tau}_w = A\left(\overline{\frac{1}{T}}\right) + B\left[\left(\overline{\frac{1}{T}}\right)^2 + \overline{\left(\frac{1}{T}\right)'^2}\right] \tag{3.1}$$

was used to fit the relationship between the time of flight T of the heat tracer and the mean skin friction $\bar{\tau}_w$. The calibration constants A and B were determined by a least-square fit. This calibration takes into account the fluctuation intensity of the skin friction (for details see Ruderich, private communication 1985). The procedure is probably similar to the calibration procedure of Eaton & Johnston (1980).

Static pressure was measured by static-pressure orifices (0.6 mm diameter) along the centreline, at various positions in spanwise direction on the splitter plate and on the bluff plate. The pressure tappings were connected to a microcomputer-interfaced micromanometer (Froebel & Vagt 1974).

4. Wall-static-pressure and skin-friction distributions

According to Roshko & Lau (1965) pressure distributions in long separation bubbles correlate well if the pressure coefficient is defined as

$$\tilde{c}_p = \frac{c_p - c_{p\min}}{1 - c_{p\min}} \tag{4.1}$$

and plotted against x/x_2. $c_p = (p - p_\infty)/(0.5\rho U_\infty^2)$ is the usual pressure coefficient and $c_{p\min}$ is defined as $(p_{\min} - p_\infty)/(0.5\rho U_\infty^2)$, where the index ∞ denotes the undisturbed

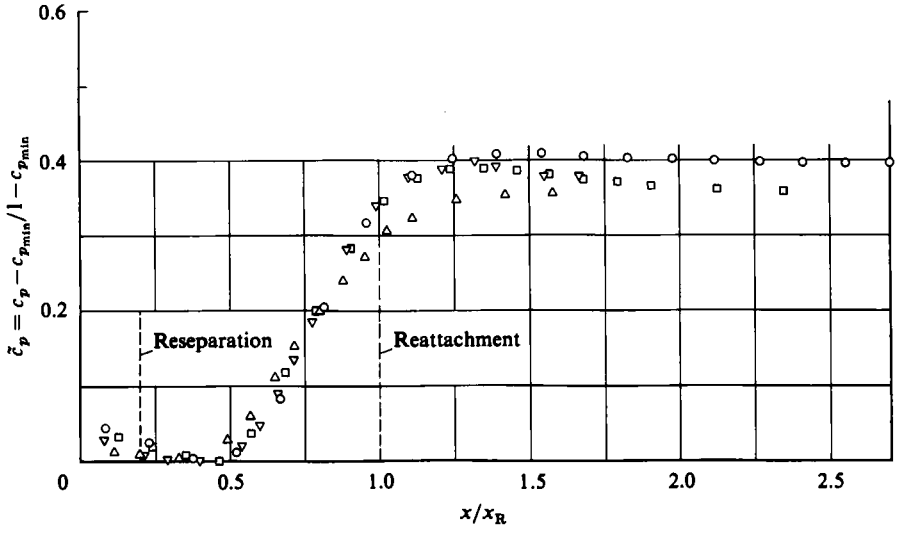

FIGURE 7. Development of the pressure coefficient in the reverse-flow region and downstream of reattachment along the centreline.

	Re_{h_F}	h_F (mm)	x_F/h_F	Blockage (%)
○	1.4×10^4	22	17.2	10
□	0.9×10^4	11	22.6	5.7
△	1.4×10^3	2.4	33.6	5 (Roshko & Lau 1965)
▽	1.35×10^4	9	23.9	2.5 (Hillier *et al.* 1983)

upstream velocity and p_{min} the minimum pressure on the splitter plate downstream of the fence. x is the distance from the sharp edge of the bluff plate ($x = 0$ mm) in streamwise direction and x_R the distance to the centre of the reattachment region on the centreline as determined both from oil-flow photographs and skin-friction measurements.

$\tilde{c}_p$ is plotted against x/x_R in figure 7 for the two fence configurations investigated here and compared with the results obtained by Roshko & Lau (1965) and Hillier *et al.* (1983) on a blunt plate. Agreement between these data is good over most of the reverse-flow region, confirming that effects due to blockage, apect ratio and free-stream turbulence ($0.1 \leqslant T_u \leqslant 0.66$) are taken into account by (4.1) (for values of these parameters see table 1). This adds weight to the assumption that x_R is in fact one basic lengthscale of this flow problem. It is different, though not much, from the length L_R of the reverse-flow region, measured between reseparation and reattachment, which for the larger of the two fences is 14.9 fence heights against 17.2 for x_R. Both x_R and L_R are apparently functions of several parameters such as: fence height; aspect ratio; angle of the separating shear layer; blockage ratio; streamwise pressure gradient; state of the boundary layer on the bluff plate; Reynolds number; free-stream turbulence level; and integral lengthscale of the oncoming flow.

Hillier (1978) has noted that the bubble length decreases with increasing turbulence level and that the effects of integral scale appear to be weak or indeterminate on bodies with sharp-edged separation. An investigation by Dziomba (experimental investigation of separating regions of bluff bodies, private communication, 1984) has shown that a pair of trip wires on the front face of a blunt plate (configuration (*b*) in figure 1) causes the boundary layer to become turbulent before it separates, reduces the base pressure downstream of separation and can shorten the reverse-flow region by 40%. The basic effect of the trip wire appears to be a change in the separation

angle due to the recirculation bubble between the trip wire and the position of separation. Nothing is known so far about the effect of an external streamwise pressure gradient on the length of the reverse-flow region, and Reynolds-number effects appear to be small if the Reynolds number is sufficiently large.

In the past the total height D of the fence, the height of the backward-facing step or the fence height h_F above the splitter plate have been used as normalizing lengthscales, but their significance is not clear and Hillier may be correct when he states that the body thickness at separation is a fairly arbitrary physical scale with which to normalize. We will use it, however, for a normalization of distances normal to the splitter plate.

Besides the pressure coefficient given above, Roshko & Lau (1965) have also defined a coefficient of reattachment-pressure rise which is a measure for the pressure difference between the lowest and the highest pressure

$$\tilde{c}_{p_m} = \frac{c_{p_{max}} - c_{p_{min}}}{1 - c_{p_{min}}}. \tag{4.2}$$

$\tilde{c}_{p_m}$ was found by Roshko & Lau to be approximately 0.36 for the separated shear layers of most configurations presented in figure 1 (see also table 1). Other pressure coefficients, e.g. Hillier *et al.* (1983), do not collapse pressure distributions significantly better than $\tilde{c}_p$ and therefore were not used.

Skin-friction distributions in reverse-flow regions downstream of bluff bodies and backward-facing steps have been measured by Castro & Dianat (1983) and Westphal, Johnston & Eaton (1984), for example. Their results agree qualitatively with our data. The skin-friction coefficient $\bar{c}_f = 2\bar{\tau}_w/\rho U_\infty^2$ along the centreline is presented in figure 8. It shows a change from positive to negative at $x/x_R = 0.13$, a minimum of -3.25×10^{-3} at $x/x_R = 0.64$, and is again zero at the centre of the reattachment region (consistent with the oil-flow picture). $\bar{c}_f$ continues to increase sharply downstream of reattachment, reaching a plateau of 3.6×10^{-3} at $x/x_R = 2.80$, which is only 10% higher than the magnitude of the extremum in the reverse-flow region.

The distribution of the r.m.s. value of the fluctuating skin-friction coefficient $\overline{(c_f'^2)}^{\frac{1}{2}} = 2\overline{(\tau_w'^2)}^{\frac{1}{2}}/(\rho U_\infty^2)$ shows a hump just upstream of reattachment ($x/x_R = 0.85$) and then falls to an approximately constant value in the attached shear layer. The ratio $\overline{(c_f'^2)}^{\frac{1}{2}}/\bar{c}_f$ at $y = 0.08$ mm, which is $\overline{(u'^2)}^{\frac{1}{2}}/\bar{u}$ in the limit $y \to 0$ (Kreplin 1976), is approximately constant for $x/x_R > 1.5$ and has a value 0.40 higher than the 0.29 which was measured in the fully developed boundary layer at the same downstream length on the splitter plate (generated without the bluff plate and an elliptical nose). It should be noted that the distribution of the r.m.s. value of c_f is qualitatively similar to that of the r.m.s. value of the static pressure as shown in figure 6 of Hillier & Cherry (1981).

Figure 8 also presents the distribution of the reverse-flow parameter χ_{τ_w} measured by the wall pulsed wire. This parameter is defined as the ratio of the samples with a negative sign and the sum of all samples (Simpson 1976) or

$$\chi_{\tau_w} = \frac{\int_{-\infty}^{0} p(\tau_w)\,\mathrm{d}\tau_w}{\int_{-\infty}^{+\infty} p(\tau_w)\,\mathrm{d}\tau_w}. \tag{4.3}$$

The χ_{τ_w} distribution shows a plateau approximately in the centre of the reverse-flow region and reaches zero only at about half a bubble length downstream from reattachment. The rather long 'tail' of the χ_{τ_w} distribution in the region of the

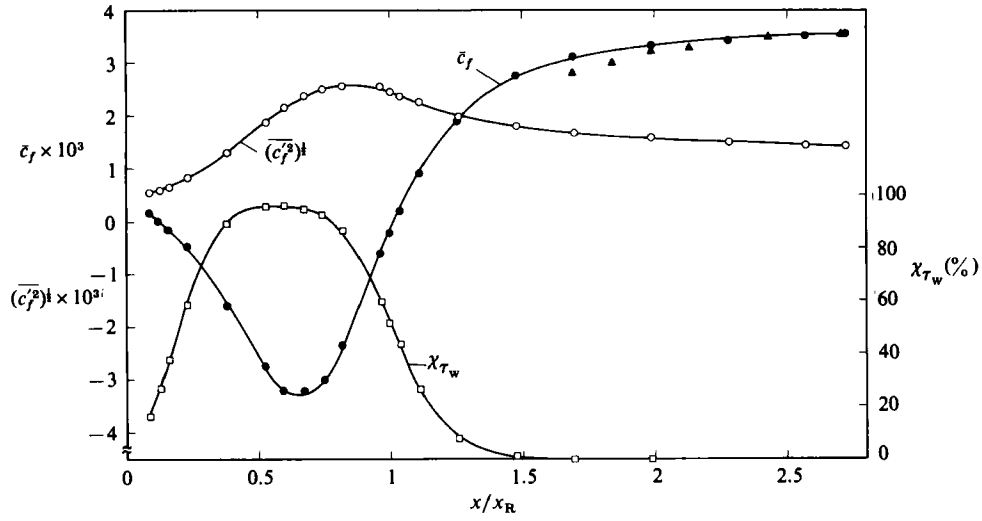

FIGURE 8. Distributions of mean skin friction, skin-friction intensity and skin-friction reverse-flow parameter $\chi_{\tau w}$ in the reverse-flow region and downstream of reattachment along the centreline ($Re_{h_F} = 1.4 \times 10^4$. □, ○, ●, wall pulsed wire; ▲, Preston tube (2 mm$^\phi$).

attached shear layer explains the discrepancies between the hot-film data, which are too high owing to rectification effects (not shown here), and those of the wall pulsed wire. Preston-tube data are erroneous because of partial reverse flow and because of the lack of a universal logarithmic law in this region of the flow.

Since the pressure coefficient suggested by Roshko & Lau (4.1) provides a good correlation of pressure distribution in long separation bubbles, a skin-friction coefficient was defined in an analogous manner,

$$\bar{c}_{f_B} = \frac{\bar{c}_f - \bar{c}_{f\min}}{2 - \bar{c}_{f\min}}, \tag{4.4}$$

and plotted against x/x_R with $\bar{c}_{f\min}$ as the minimum value of the friction coefficient in the reverse-flow region (figure 9). The second distribution ($Re_{h_F} = 0.9 \times 10^4$) was measured downstream of the smaller bluff plate ($h_F = 11$ mm). Owing to the smaller fence height the distance to reattachment was reduced by 33%. Nevertheless agreement between these two cases is very good.

5. Three-dimensional effects

The oil-flow pictures (cf. figure 4) have shown that there are three-dimensional effects in the reverse-flow region and, owing to the curved reattachment region, immediately downstream of reattachment. The strength of these effects and their extension toward the centreline of the flow were investigated by measurement of various quantities in the spanwise direction: static pressure; skin friction; mean velocity; r.m.s. values of the fluctuating component u' and of the correlation coefficient $R_{11}^{(3)}$ (defined below).

It has been well known from earlier investigations (e.g. Fernholz & Vagt 1981) that spanwise distributions of static pressure are often a rather insensitive indicator of secondary flows. This is confirmed again by the present measurements, where static pressure was measured at three positions ($x/x_R = 0.027; 1.35; 2.95$) across the splitter

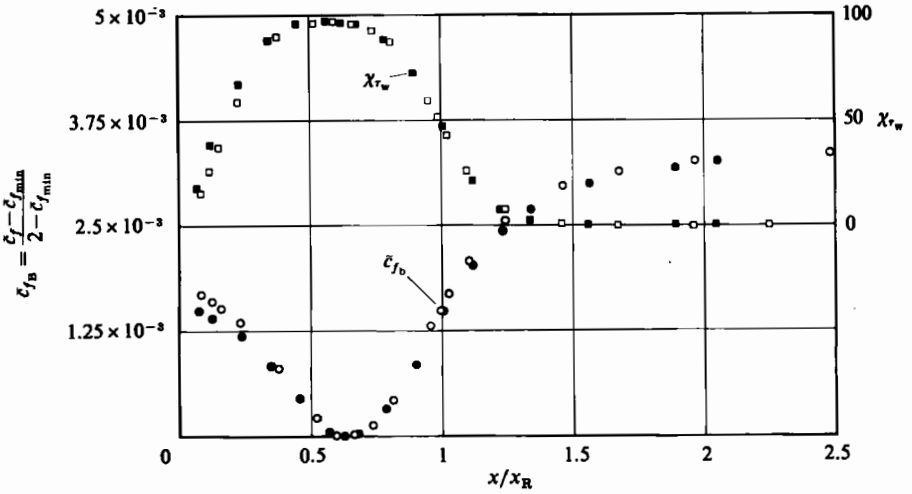

FIGURE 9. Development of the skin-friction coefficient $\bar{c}_{f_B}$ and the reverse-flow parameter $\chi_{\tau w}$ in the reverse-flow region and downstream of reattachment along the centreline.

		Re_{h_F}	$1000 \times \bar{c}_{f\min}$	x_R/h_F
○	□	1.4×10^4	−3.27	17.2
●	■	0.9×10^4	−2.87	22.6

plate. Within a range of $-0.8 \leqslant z/(\frac{1}{2}w) \leqslant +0.8$ static pressure varied by at most $\pm 2\,\%$ at the first and by $\pm 0.5\,\%$ at the two downstream stations, which is almost in the uncertainty range of such measurements.

Figure 10 presents spanwise skin-friction distributions in the reverse-flow region ($x/x_R = 0.52$), just downstream of $x/x_R = 1.48$ and far downstream of reattachment ($x/x_R = 2.72$), plotted against $z/(\frac{1}{2}w)$, where w is the width of the tunnel. These data were obtained using a Preston tube and are qualitative only for the first and second positions. As may be expected from the oil-flow pattern, there is hardly any variation over the core region ($\pm 20\,\%$) of the span in the centre of the reverse-flow region. This is due to the fairly straight section of the reattachment region in the vicinity of the centreline which assures uniform starting conditions for the near-wall flow in the reverse-flow region.

The skin-friction distribution at $x/x_R = 1.48$ reflects the curvature of the reattachment region. $\bar{\tau}_w$ is larger by $30\,\%$ towards the tunnel sidewall since reattachment occurs further upstream than on the centreline. Consequently the uniform centre region is narrower and extends only $\pm 10\,\%$ on both sides of the centreline. At $x/x_R = 2.72$ the increase of skin friction towards the tunnel sidewall is reduced to about $14\,\%$ above the centreline value, resulting in an almost uniform spanwise behaviour over most of the splitter plate. In all three cases the symmetry of the spanwise skin-friction distribution is remarkable.

Figure 11 presents spanwise distributions of the mean velocity $\bar{u}$ and the Reynolds normal stress $\overline{u'^2}$ made dimensionless by the respective centreline values at two heights above the splitter plate in the reverse-flow region. The mean velocity values are constant to within $\pm 15\,\%$ over the width of the $\bar{\tau}_w$ plateau, falling to $60\,\%$ of the centreline value towards the sidewalls at $y/h_F = 0.66$. At $y/h_F = 2.20$ there is a sharp increase towards the tunnel sidewalls, possibly due to the influence of the horseshoe vortices. These measurements were supplemented by distributions of the reverse-

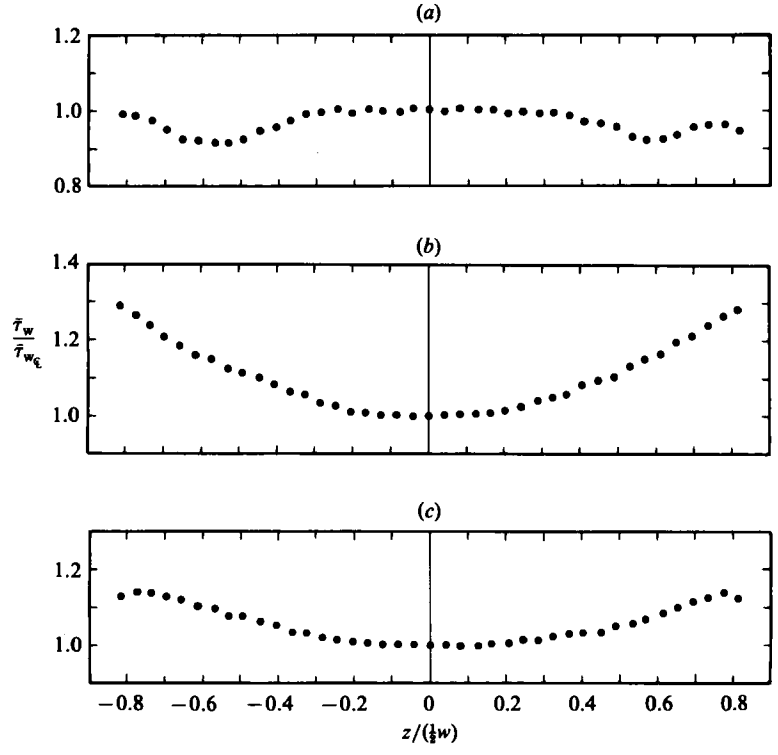

FIGURE 10. Skin-friction distribution in the spanwise direction on the splitter plate at different positions x/x_{R} along the centreline ($\frac{1}{2}w = 245$ mm, Preston tube 1 mm dia. $Re_{h_{\mathrm{F}}} = 1.4 \times 10^4$). (*a*) $x/x_{\mathrm{R}} = 0.52$; (*b*) 1.48; (*c*) 2.72.

flow-factor χ by a pulsed-wire probe. Figure 12 shows that χ is approximately 92 % near the wall in the centre part of the reverse-flow region and that it falls to 78 % towards the tunnel sidewalls. This indicates that about 20 % of the samples outside the centre region represent flow in the downstream direction.

Further information about the spanwise behaviour of the flow may be obtained from measurements of the spanwise correlation coefficients, for example from $R_{11}^{(3)} = \overline{u'u'_{\Delta z}}/[(\overline{u'^2})^{\frac{1}{2}}(\overline{u'^2_{\Delta z}})^{\frac{1}{2}}]$ and from the integral lengthscale Λ_z which is the value of the positive area between the axes and the $R_{11}^{(3)}$ curve. These measurements were performed by means of two normal hot-wire probes with the wires aligned in the y-direction so that data at close distances between the probes could also be obtained. Checks with the wires in z-direction showed that the direction of the wire affected the measured values very little.

Figure 13 presents distributions of the spanwise correlation coefficient $R_{11}^{(3)}$ in the reverse-flow region ($x/x_{\mathrm{R}} = 0.38$) and downstream of reattachment ($x/x_{\mathrm{R}} = 1.26$). The caption gives the integral lengthscales Λ_z at these positions and additionally at $x/x_{\mathrm{R}} = 2.69$. Here the $R_{11}^{(3)}$ distributions again fall on one curve but were not plotted for reasons of brevity. The measurements were performed at fixed heights y_{fp} above the splitter plate at four locations z_{fp} in spanwise direction in regions of the flow where changes of Λ_z in the y-direction were small. The choice of the y-position was rather arbitrary in the investigations of Kiya & Sasaki (1983) and Cherry *et al.* (1984) but is important in so far as changes of Λ_z with distance normal to the wall can vary by a factor of at least 8 (cf. profiles of Λ_z in figure 14).

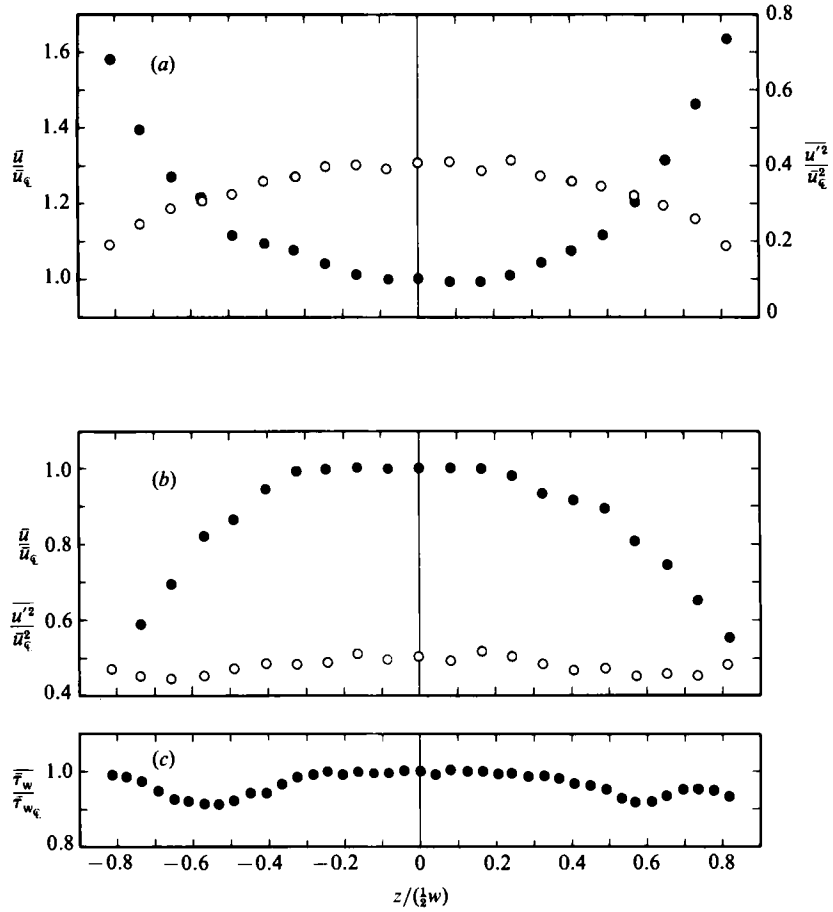

FIGURE 11. Distribution of mean skin friction, mean velocity and Reynolds normal stress in the spanwise direction at $x/x_{\mathrm{R}} = 0.52$, the latter at two positions above the splitter plate ($Re_{h_{\mathrm{F}}} = 1.4 \times 10^4$, $h_{\mathrm{F}} = 22$ mm): ●, $\bar{u}/\bar{u}_{\mathrm{e}}$; ○, $\overline{u'^2}/\bar{u}_{\mathrm{e}}^2$. (*a*) $y/h_{\mathrm{F}} = 2.20$; (*b*) 0.66; (*c*) 0.

Figure 13 shows that the distributions of $R_{11}^{(3)}$ are similar in spanwise direction at fixed locations x/x_{R} and y and that consequently Λ_z hardly changes along the span (cf. caption of figure 13). Λ_z increases along the centreline from $\Lambda_z/h_{\mathrm{F}} = 0.36$ at $x/x_{\mathrm{R}} = 0.38$ to 0.73 at $x/x_{\mathrm{R}} = 1$ and to 1.14 at $x/x_{\mathrm{R}} = 2.69$. This is a monotonic increase of Λ_z in the downstream direction following approximately the locus of $(\overline{u'^2})_{\max}$ (see figure 14). The increase of Λ_z is larger in the mixing layer than in the region downstream of reattachment.

Taking into account the flow-visualization photographs (e.g. figure 3) one may conclude that the long spanwise coherent structures just downstream from separation have broken up into rather short structures at $x/x_{\mathrm{R}} = 0.35$ but then grow again in spanwise direction as the flow proceeds downstream. The size of the coherent structures in the spanwise direction, as characterized by Λ_z, increases towards the high-speed side of the curved shear layer (figure 14). Following the locus of $(y/h_{\mathrm{F}})_{T_{u=10\%}}$ in the downstream direction, one may notice that Λ_z is largest upstream of reattachment and then decreases, becoming approximately uniform normal to the wall at $x/x_{\mathrm{R}} = 2.69$. The different sizes of the coherent structures on the two sides of the mixing layer may be explained by the different interaction mechanisms

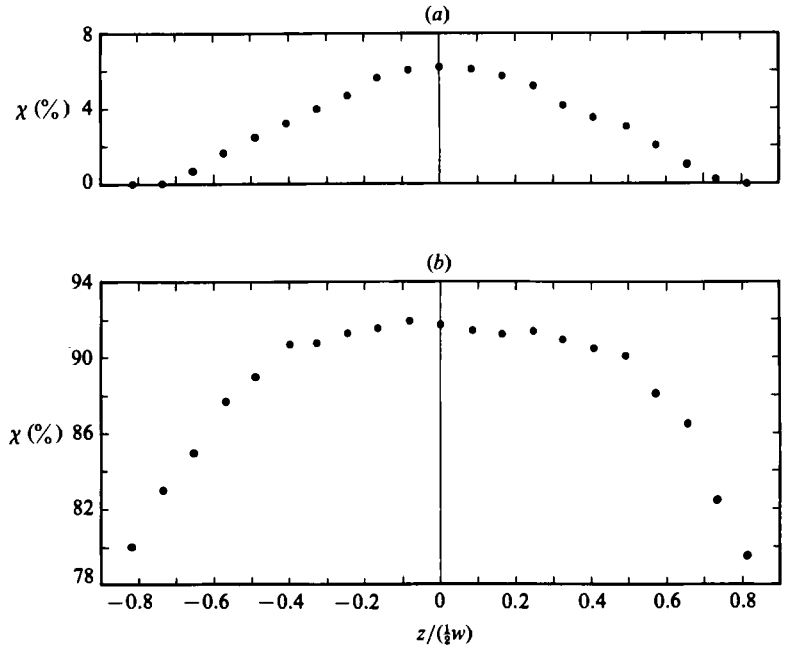

FIGURE 12. Distribution of the reverse-flow parameter χ in spanwise direction at $x/x_R = 0.52$ and two positions y above the splitter plate ($Re_{h_F} = 1.4 \times 10^4$). (*a*) $y/h_F = 2.20$; (*b*) 0.66.

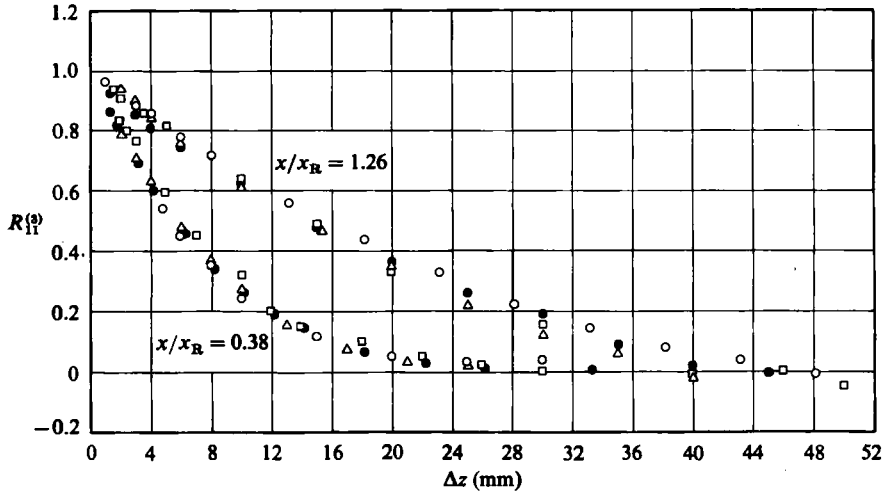

FIGURE 13. Distributions of the spanwise correlation coefficient $R_{11}^{(3)}$ in the reverse-flow region and downstream of reattachment ($Re_{h_F} = 1.4 \times 10^4$).

z_{fp}	0	30	60	120	x/x_R	y_{fp}
(mm)	○	●	□	△	—	(mm)
Λ_z (mm)	8	8	8	8	0.38	53
Λ_z (mm)	18	16	17	16	1.26	40
Λ_z* (mm)	25	—	23	22	2.69	65

fp = fixed probe.
* $R_{11}^{(3)}$ = distributions not shown.

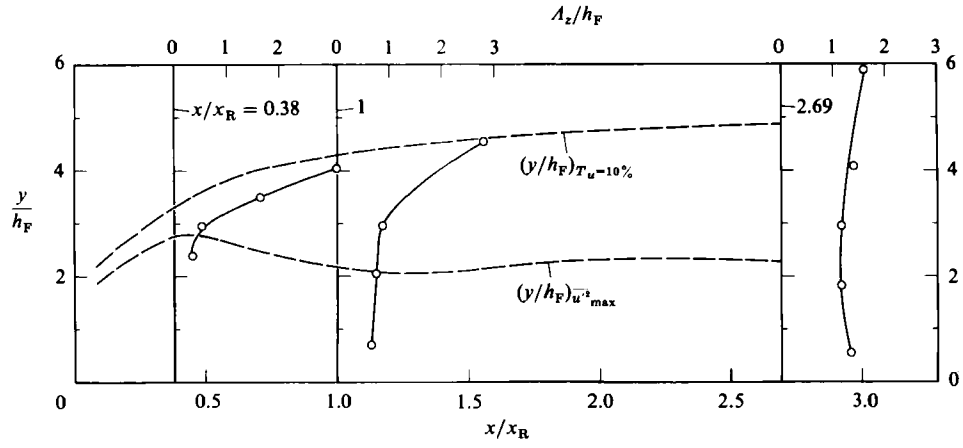

FIGURE 14. Distributions of the integral lengthscale Λ_z in normal direction to the splitter plate at three positions x/x_R along the centreline ($Re_{h_F} = 1.4 \times 10^4$).

between the outer flow on the one side and the reverse-flow region on the other. In the latter case the interaction is much stronger, leading to shorter spanwise lengthscales which increase when the influence of the bubble on the shear layer decreases (see also the discussion of the spreading rate below).

A comparison with measurements in the blunt-plate flow (Kiya & Sasaki 1983) gives the same qualitative result but does not show the decrease of Λ_z in the outer region downstream of reattachment, since measurements in this region were not presented. The measurements of the integral lengthscales in the spanwise direction are supplemented by those in the normal direction, which will be discussed in §6.

6. Measurements in the flow field

Figure 15 shows a sequence of mean-velocity profiles through the reverse-flow and reattachment region into the attached shear layer. Full circles indicate pulsed-wire data and open circles hot-wire measurements. The latter include error estimates for high-turbulence effects using a series expansion (Vagt 1979) with the modification that $\overline{w'^2}$, which was not known everywhere, was replaced by $\overline{u'^2}$. The most obvious features are velocity maxima and minima of the profiles in the reverse-flow region and their rather fast disappearance in the attached flow. The maximum velocity remains everywhere higher than the upstream velocity U_∞, which is indicative of the blockage effect of the flow. The uncertainty range of these measurements varies according to the flow region but is estimated to be 5–10 % in the reverse flow and 2 % outside it.

6.1. *The reverse-flow region*

Since there are very few measurements of velocities in a reverse-flow region it seemed appropriate to investigate this part of the flow, which is driven by the pressure difference between reattachment and the pressure minimum in the reverse-flow region, in more detail. A typical set of profiles, obtained in approximately the centre of the reverse-flow region ($x/x_R = 0.52$), is shown in figure 16 and plotted in physical coordinates against the distance y normal to the wall. The semi-logarithmic scale was chosen to enlarge the near-wall region. The measurements comprise the mean

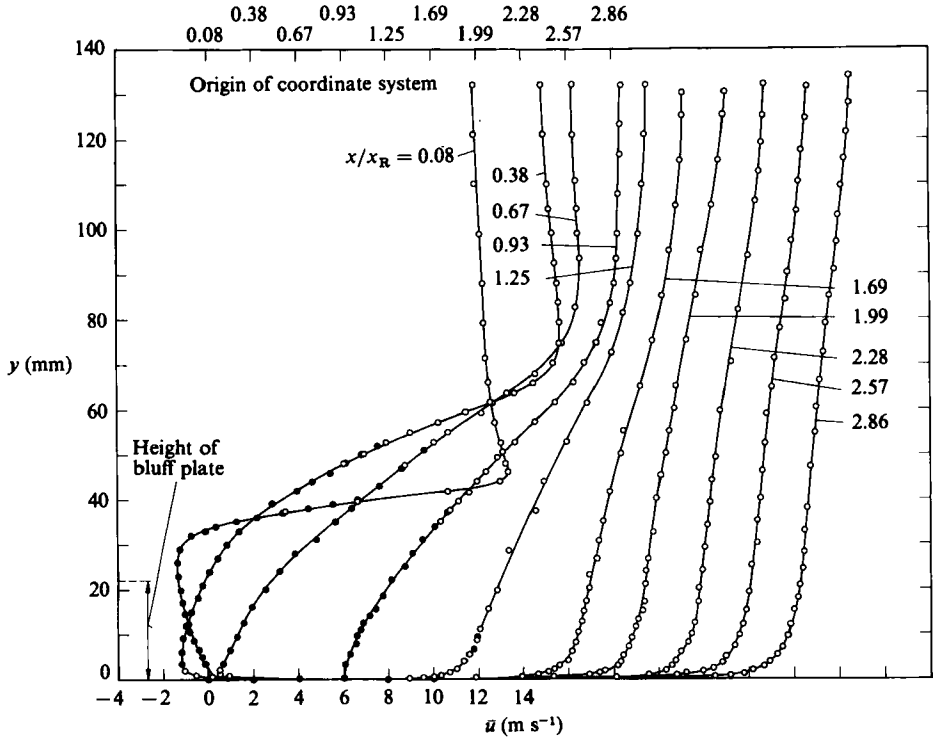

FIGURE 15. Mean-velocity distribution downstream of the bluff plate along the centreline of the splitter plate ($Re_{h_F} = 1.4 \times 10^4$): ○, hot-wire (H.W.) data (error estimates due to Vagt); ●, pulsed-wire (P.W.) data.

velocity $\bar{u}$, the r.m.s. value of the fluctuating velocity u', the turbulence intensity $T_u = \overline{(u'^2)}^{\frac{1}{2}}/|\bar{u}|$ and the reverse-flow parameter χ. Data were obtained by means of a miniaturized pulsed-wire probe from 3.5 mm normal to the wall, by a large pulsed-wire probe (PELA size probe) with an upper velocity limit of about 18 m/s (instantaneous velocity) in the mixing layer and by hot-wire probes. Measurements by the latter probes were, however, used only if χ was below 10% or above 90%, otherwise systematic errors would have been too large, as is obvious from figure 16.

Mean velocity measurements are presented as open circles (hot-wire data) and as full circles (pulsed-wire data). When the flow was unidirectional error estimates of $\bar{u}$ due to the high turbulence level were at most 11%. As is to be expected, differences between the data obtained by the two techniques are large in flow regions where χ is between 10 and 90%, with the hot-wire measurements being too high because of rectification effects. In the reverse-flow region the u' data differ by at most 15% if measured by the hot wire and the pulsed wire, respectively. The turbulence intensity T_u is 40% and almost constant in the near-wall region. The mean velocity reaches 30% of the maximum velocity, and the r.m.s. value about 50% of the respective maximum values in the separated shear layer. The cross-over point where the mean velocity $\bar{u}$ changes sign is at $y/h_F = 1.50$ in this profile and the distribution of the locus $(y/h_F)_{\bar{u}=0}$ in streamwise direction is shown in figure 19.

Mean velocity and skin-friction measurements combined permit the plotting of the velocity profile in near-wall coordinates, $|\bar{u}|/u_\tau$ against yu_τ/ν, with $u_\tau = (|\bar{\tau}_w|/\rho)^{\frac{1}{2}}$ as the skin-friction velocity, and the checking of the validity of the law of the wall in

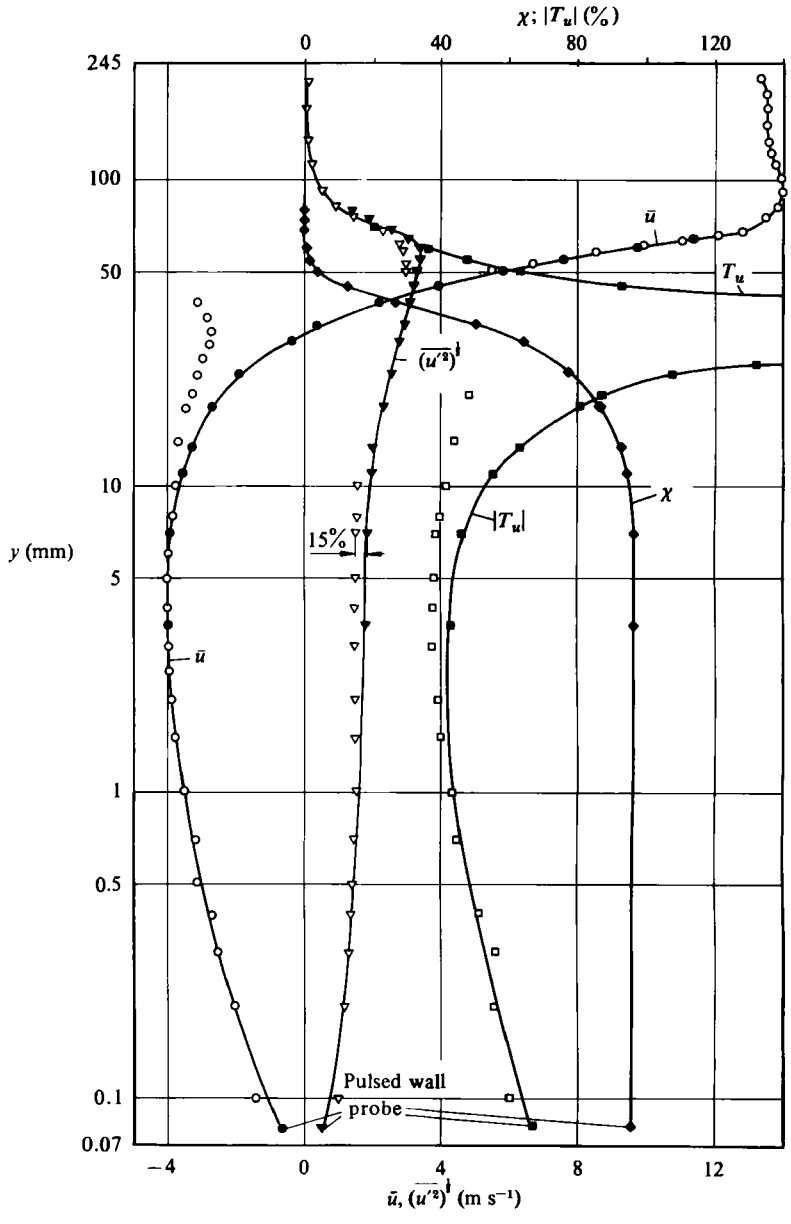

FIGURE 16. Distributions of mean velocity, fluctuating velocity, turbulence intensity T_u, and reverse-flow parameter χ in the reverse-flow region ($x/x_R = 0.524$, $Re_{h_F} = 1.4 \times 10^4$): ▽, ○, □, hot-wire (H.W.) probe; ◆, ▼, ●, ■, pulsed-wire (P.W.) probe.

the reverse-flow region. Among the seven measured velocity profiles we have chosen three for which the reverse-flow parameter was closest to 100%. They are presented in figure 17 and demonstrate that the logarithmic law of the wall (compare with the straight line in figure 17) does not hold. The discrepancies between the straight line and the measured data are not reduced if error estimates are included for the high level of turbulence. Agreement with the linear law in the viscous sublayer is good.

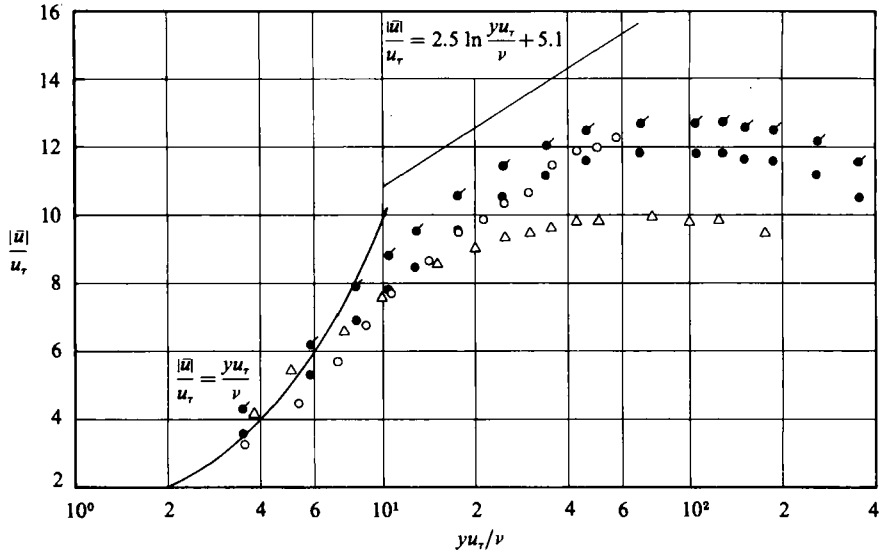

FIGURE 17. Near-wall mean-velocity distributions in the reverse-flow region (u_τ from wall pulsed wire, $\bar{u}$ from H.W. and P.W.).

	x/x_R	u_τ (m s^{-1})	χ_w (%)	
○	0.38	0.268	90	(Modified 'Vagt' error estimate)
●	0.52	0.352	96	
△	0.67	0.379	95	

◐, raw data

6.2. *Development of fluctuating quantities*

In an 'ordinary' plane mixing layer the maxima of Reynolds normal and shear stresses, non-dimensionalized by the maximum velocity $\bar{u}^2_{max}$ or the upstream velocity u^2_∞, reach limiting values in the self-similar region (e.g. Wygnanski & Fiedler 1970). This is not so in the separated shear layer generated in the present experiment, as shown in figure 18. All curves of the maxima of the fluctuating quantities reach a maximum in the second half of the reverse-flow region and then fall below their starting values in the attached-flow region. The Reynolds normal stresses are very much higher than in other separated shear layers over the whole flow region and demonstrate the high turbulence level of this flow.

For a comparison with other separated shear flows – an attaching single-stream mixing layer (Wood & Bradshaw 1984), a blunt plate flow (Kiya & Sasaki 1983), and a plane single-stream mixing layer (Wygnanski & Fiedler 1970) – the values of the absolute maxima are given in table 2. These data may serve only for an order-of-magnitude comparison, since both the flows and the measuring techniques were different (pulsed wire, hot wire and split film). The kind of measuring technique applied could be important for the first three cases quoted in table 2 because some data were taken close to, or at, reattachment with a very high turbulence level $(\overline{u'^2})^{\frac{1}{2}}_{max}/\bar{u}$ and instantaneous reverse flow. As for the uncertainty of our data in this region only the $\overline{u'^2}$ values, measured by means of the pulsed wire, are regarded as being correct whereas the $\overline{v'^2}$ and $\overline{u'v'}$ data measured by hot wires could be too low, although LDV measurements by Stevenson *et al.* (1984) behind a backward-facing step give the maximum value of $|\overline{u'v'}/u^2_\infty|$ as 0.02, which is the same as the largest values in table 2.

Figure 19 shows the loci of the maxima of the quantities given in figure 18. They

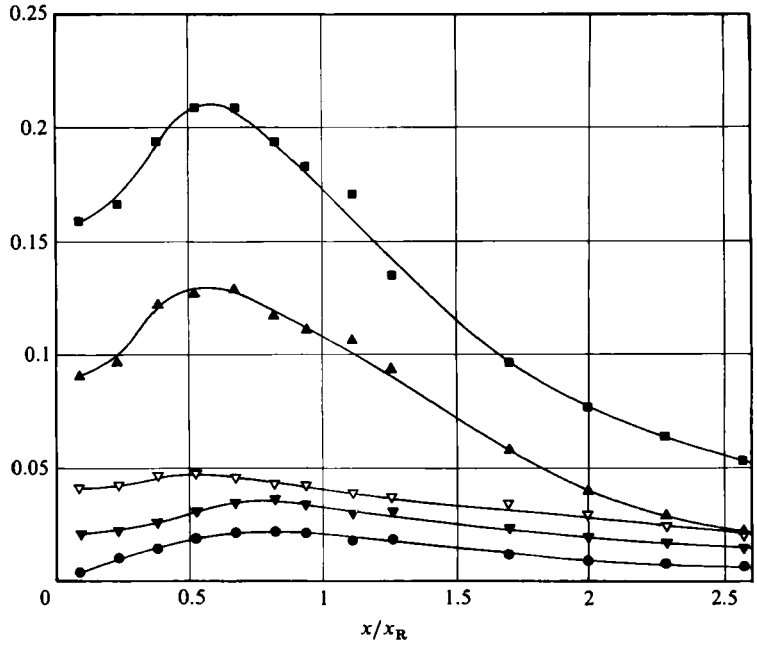

FIGURE 18. Development of maxima of fluctuating quantities in the mixing layer and downstream from reattachment along the centreline ($Re_{h_F} = 1.4 \times 10^4$): ■, $\overline{q'^2_{max}}/u^2_\infty$; ▲, $\overline{u'^2_{max}}/u^2_\infty$; ▼, $\overline{v'^2_{max}}/u^2_\infty$; ▽, $\overline{w'^2_{max}}/u^2_\infty$; ●, $\overline{u'v'_{max}}/u^2_\infty$.

	$\frac{\overline{u'^2_{max}}}{u^2_\infty}$	$\frac{\overline{v'^2_{max}}}{u^2_\infty}$	$\frac{\overline{w'^2_{max}}}{u^2_\infty}$	$\frac{\overline{q'^2_{max}}}{u^2_\infty}$	$\frac{\overline{u'v'_{max}}}{u^2_\infty}$	$\frac{\overline{u'v'_{max}}}{q'^2_{max}}$	$\frac{(\overline{u'^2})^{\frac{1}{2}}_{max}}{\bar{u}}$ (%)
Present experiment	0.116	0.032	0.041	0.193	0.020	0.10	48
Wood & Bradshaw	0.030	0.019	0.019	0.068	0.011	0.16	33
Kiya & Sasaki	0.044	0.020	0.032	0.096	0.021	0.22	25
Wygnanski & Fiedler	0.031	0.019	0.023	—	0.009	—	17.6

TABLE 2

are at about the same height above the splitter plate and the position of their 'joint locus' is between 2 and 2.7 h_F in the reverse-flow region. It could be used as a scaling length in the y-direction. Downstream from reattachment the curves no longer collapse on to but separate from each other, with the curve for $\overline{w'^2_{max}}$ being the lowest. If the locus of $\overline{u'^2_{max}}$ is interpreted as the centre of the separated shear layer (Kiya & Sasaki 1983) this maximum falls on the 'mean reattachment streamline ($\psi = 0$)' in the range $0 \leqslant x/x_R \leqslant 0.5$ along the centreline. This latter streamline together with the separation streamline ($\bar{u} = 0$) may serve as a guide for other measurements.

A scaling velocity often used in investigations of two-stream plane mixing layers (e.g. Brown & Roshko 1974) is the velocity difference $\Delta\bar{u}$ between the maxima of the mean velocities of the two flows forming the mixing layer. For the present experiment

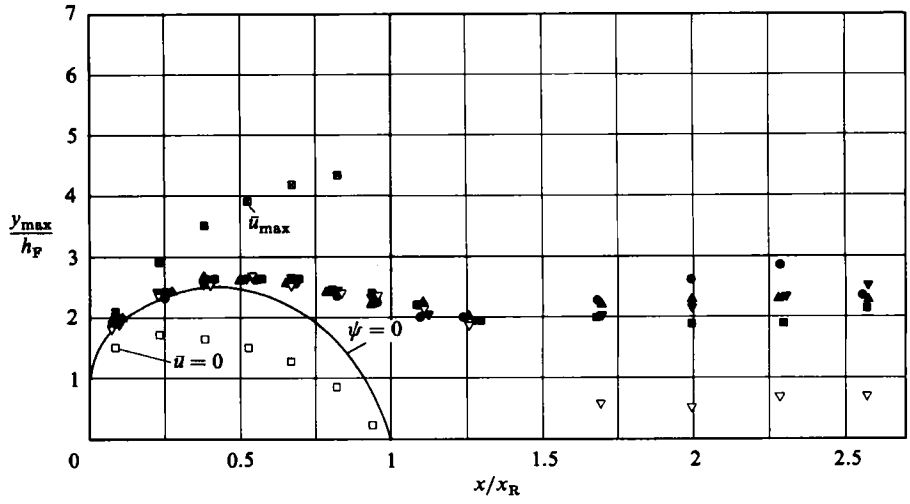

FIGURE 19. Development of the position of the maximum of various quantities in the mixing layer and downstream of reattachment along the centreline ($Re_{h_F} = 1.4 \times 10^4$): ⊠, $(y/h_F)_{\bar{u}_{max}}$; □, $(y/h_F)_{\bar{u}=0}$; ■, $(y/h_F)_{\overline{q^2}_{max}}$; ▲, $(y/h_F)_{\overline{u^2}_{max}}$; ▼, $(y/h_t)_{\overline{v^2}_{max}}$; ▽, $(y/h_F)_{\overline{w^2}_{max}}$; ●, $(y/h_F)_{\overline{u'v'}_{max}}$.

$\Delta\bar{u}$ was calculated from the maximum velocity in the separated shear layer $\bar{u}_{max}$ and the maximum velocity of the reverse-flow $\bar{u}_{min}$. Owing to displacement effects $\bar{u}_{max}$ increases over u_∞, and owing to the reverse-flow $\bar{u}_{min}$ reaches values of about $0.3\bar{u}_{max}$. Thus $\Delta\bar{u}$ increases, leading to a different distribution of the dimensionless maxima of the fluctuating quantities (figure 20) as if they were made dimensionless by u_∞. A comparison between figures 18 and 20 shows that the relative minima in the reverse-flow region and the shift of the maxima close to reattachment are due only to the changes in $\Delta\bar{u}$.

The distributions of $\bar{u}_{max}$ and $\bar{u}_{min}$ also influence the spreading rate of the separated shear layer, expressed by the vorticity thickness δ_ω. It was defined by Brown & Roshko (1974) as

$$\delta_\omega = \frac{\bar{u}_{max} - \bar{u}_{min}}{(\partial\bar{u}/\partial y)_{max}} = \frac{\Delta\bar{u}}{(\partial\bar{u}/\partial y)_{max}}, \tag{6.1}$$

where $(\partial\bar{u}/\partial y)_{max}$ was determined on the side facing the splitter plate. δ_ω/x_R (with $x_R = 376$ mm) is plotted against x/x_R in figure 21 and, if the first data point at $x/x_R = 0.085$ is disregarded, increases linearly to the end of the reverse-flow region. Then the slope changes sharply owing to the decreasing values of $(\partial\bar{u}/\partial y)_{max}$.

The slope $d\delta_\omega/dx$ equals 0.148 compared with that of 0.18 (average value for several experiments, e.g. Eaton & Johnston 1980) for a single-stream plane mixing layer. The values of δ_ω/x_R obtained by Eaton & Johnston (1980) downstream of a backward-facing step are given for comparison and agree well with our data (figure 21) despite the different flow configurations.

For purposes of comparison, figure 21 also shows the growth of the maximum slope thickness δ_{ms} (here $\bar{u}_{max}$ is used in the definition instead of $\Delta\bar{u}$), which was determined by Cherry *et al.* (1984) and compared with flow data of similar geometries. The ratio of δ_ω and δ_{ms} is a measure of the ratio of $\Delta\bar{u}$ and $\bar{u}_{max}$, which reaches a maximum value of 1.31 approximately in the centre of the reverse-flow region.

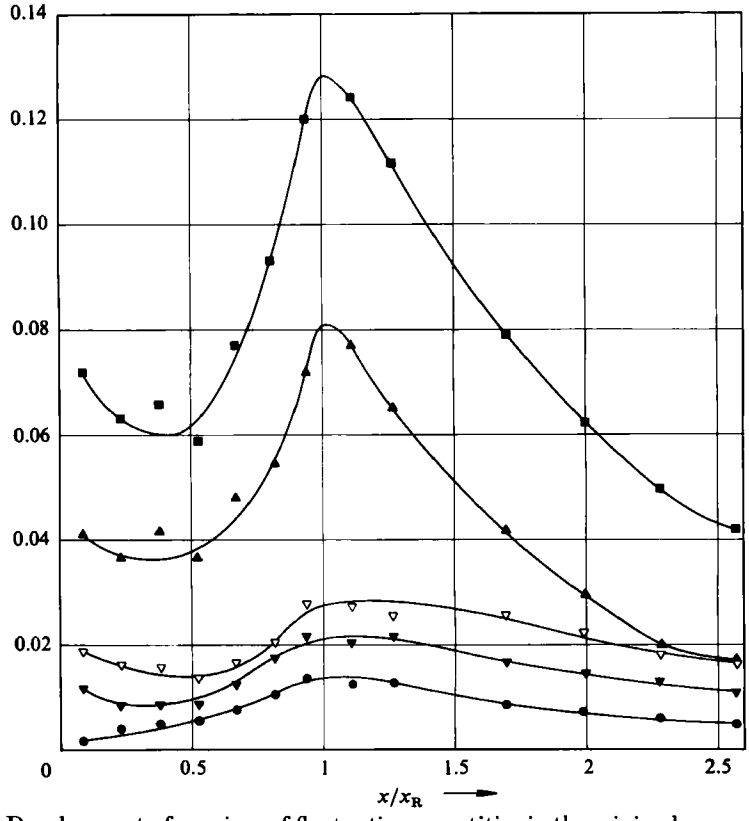

FIGURE 20. Development of maxima of fluctuating quantities in the mixing layer and downstream of reattachment along the centreline ($Re_{h_F} = 1.4 \times 10^4$): ■, $\overline{q'^2_{max}}/\Delta\bar{u})^2$; ▲, $\overline{u'^2}/\Delta\bar{u}^2$ (P.W.); ▼, $\overline{v'^2_{max}}/(\Delta\bar{u})^2$ (H.W.); ▽, $\overline{w'^2_{max}}/(\Delta\bar{u})^2$ (H.W.); ●, $\overline{u'v'_{max}}/(\Delta\bar{u})^2$ (H.W.).

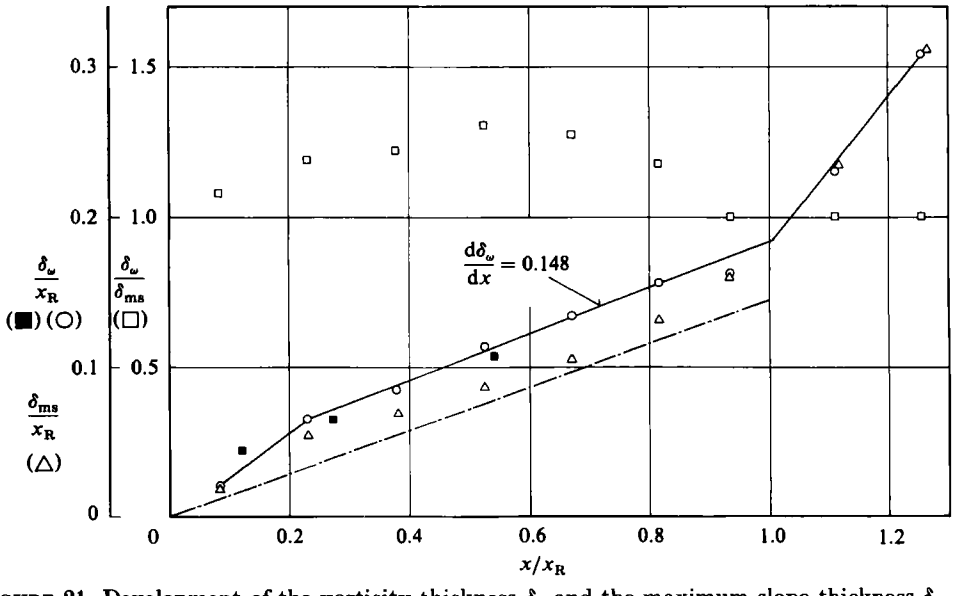

FIGURE 21. Development of the vorticity thickness δ_ω and the maximum slope thickness δ_{ms} for the separated and attached shear layer along the centreline ($Re_{h_F} = 1.4 \times 10^4$). ——, P.W. data; – – –, measurements of δ_{ms} Cherry *et al.* (1984); ■, measurements of Eaton & Johnson (1980); ○, ■, δ_ω/x_R; △, δ_{ms}/x_R; □, $\delta_\omega/\delta_{ms}$.

6.3. *Similarity of mean and fluctuating flow quantities*

It is well known that a plane mixing layer formed by two flows with velocities u_1 and u_2 approaches similarity in the variable y/x at sufficiently high Reynolds numbers based on x. Wygnanski & Fiedler (1970) have shown, for example, that, in the self-similar region of the plane mixing layer, mean velocity, Reynolds shear stress and Reynolds normal stresses collapse on one curve if they are made dimensionless by the same reference velocity and plotted against the same dimensionless lengthscale. $\bar{u}_{\max}$ or $0.5\bar{u}_{\max}$, which is easier to determine downstream from reattachment, would be an appropriate reference velocity $\bar{u}_{\mathrm{ref}}$ and $(y-y_{\mathrm{ref}})/x$ the dimensionless lengthscale for the present flow. Here y_{ref} denotes the locus of $\bar{u}_{\mathrm{ref}}$. P.W. in figure 22 gives the position below which only pulsed-wire data were used. The distance downstream of separation is indicated by the ratio x/h_{F} instead of x/x_{R}. For convenience, both coordinates are presented in table 3.

The mean velocity profiles (figure 22) are already self-similar at $x/h_{\mathrm{F}} = 4$ (the profile at $x/h_{\mathrm{F}} = 1.5$ (open squares) deviates from the common curve) and remain so down to $x/h_{\mathrm{F}} = 19$, which is downstream of reattachment. This means that the mean-velocity profiles become self-similar further upstream than the fluctuating quantities and remain so for a longer distance, as may be seen from a comparison of figures 22 and 23. Figure 23 presents the self-similar profiles of the fluctuating quantities $\overline{q'^2}$, $\overline{u'^2}$ and $\overline{u'v'}$, again non-dimensionalized by $0.5\bar{u}_{\max}$ as $\bar{u}_{\mathrm{ref}}$. They are found to be self-similar over the range $11.5 \leqslant x/h_{\mathrm{F}} \leqslant 16$, which is much shorter than the self-similar range of the mean-velocity profiles. On the side of the mixing layer facing the splitter plate, i.e. for negative values of the abscissa, only those data are given where the reverse flow was below 10%. Self-similar behaviour of the flow in the mixing layer upstream of reattachment was also observed by Chandrasuda & Bradshaw (1981), but with larger discrepancies between profiles. The length of the self-similar region is, of course, dependent on the permitted range of discrepancies between the individual profiles of a specific type (cf. Wood & Bradshaw 1983).

A word about the uncertainty of the data may be appropriate here. In this highly turbulent flow region ($T_{u_{\max}} \to \infty$) no absolute values for the uncertainty can be given, and even error estimates as presented by Tutu & Chevray (1975) are of little help, since the assumptions for their estimates are valid only for a few points of the flow field. The uncertainty of the u' data measured by the pulsed wire is estimated to be $\pm 5\%$. Since $\overline{v'^2}$ and $\overline{w'^2}$ are less accurate than $\overline{u'^2}$ but add up to only about 50% of the $\overline{u'^2}$ (cf. figure 18) and thus contribute about 25% of $\overline{q'^2}$, we estimate the uncertainty of the fluctuating kinetic energy to be about $\pm 15\%$.

If one is prepared to accept a less general similarity concept than self-similarity, that of 'profile similarity' may be used instead. Profile families are defined as showing profile similarity if individual profiles collapse on a single curve. This is achieved by making the profile data dimensionless by the respective maximum value and by plotting them against $(y-y_{\max})/x$, where $y_{\max}$ is the locus of the maximum. For the mean velocity the profiles have been presented in figure 22 (but with $0.5\bar{u}_{\max}$); those of the fluctuating kinetic energy $\overline{q'^2} = (\overline{u'^2}+\overline{v'^2}+\overline{w'^2})$ are shown in figure 24. These latter profiles show 'profile similarity' both in the separated shear layer above the reverse-flow region and in the attached shear layer down to the end of the splitter plate. The same holds for the Reynolds normal stresses (not shown here) and for the Reynolds shear stress in figure 25, although these latter profiles have already departed from profile similarity at $x/h_{\mathrm{F}} = 34$.

Figures 26(*a*) and (*b*) show respectively the third-order and fourth-order moments

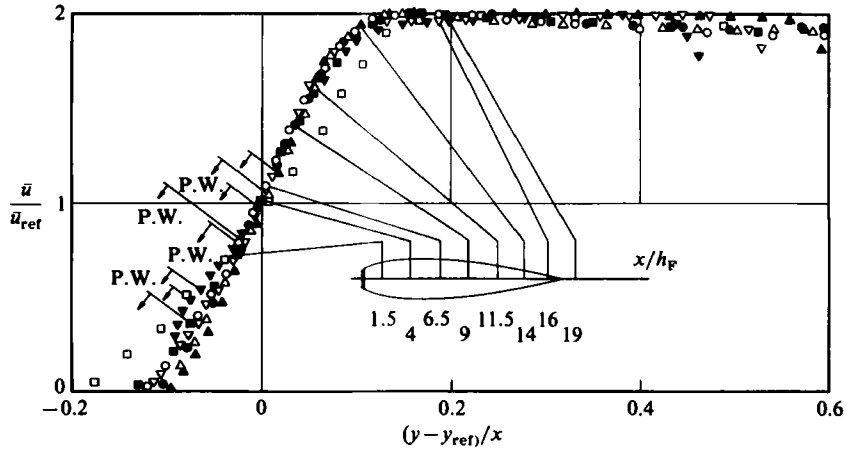

FIGURE 22. Development of the mean-velocity profiles in a curved shear layer bounding a closed reverse-flow region ($Re_{h_F} = 1.4 \times 10^4$). H.W. and P.W. data.

x/h_F	1.5	4	6.5	9	11.5	14	16
x/x_R	0.085	0.23	0.37	0.52	0.67	0.81	0.93
x/h_F	17	19	21.5	29	34	39	49
x/x_R	0.99	1.11	1.26	1.69	1.99	2.28	2.86

TABLE 3

of u' again non-dimensionalized by their respective maxima and measured by the pulsed-wire technique. Even these higher-order moments confirm profile similarity in the separated shear layer.

The similarity plot of the Reynolds-shear-stress profiles hides the large changes in the shear-stress distribution, which are more clearly seen if the profiles are plotted in physical coordinates (figure 27). Some indication of the reliability of the near-wall data downstream of reattachment is, at least, provided by the skin-friction velocity u_τ given in the right-hand plot. u_τ^2 agrees well with the near-wall Reynolds-shear-stress data for $x/h_F > 21$.

A note of caution is necessary here about the accuracy of the $\overline{u'v'}$ profiles in those regions of the flow where instantaneous reverse flow occurs. For the profiles concerned (figure 27) we have presented values of the reverse-flow factor that give an impression of the reliability of the data which – although the distributions look smooth and plausible – cannot show more than a qualitative behaviour if instantaneous reverse flow occurs or if the turbulence level is very high even without instantaneous reverse flow, as is the case here.

In general, the maxima of the profiles increase by about a factor of 7 in the separated shear layer and then decrease by a factor of 4 at the position $x/h_F = 49$, which is about 2.8 reattachment lengths downstream. The shape of this Reynolds-shear-stress profile does not resemble at all that in an equilibrium zero-pressure-gradient boundary layer, where the peak would lie very close to the wall. Such discrepancies between the two flows are confirmed by the distributions of the Reynolds normal stresses shown below.

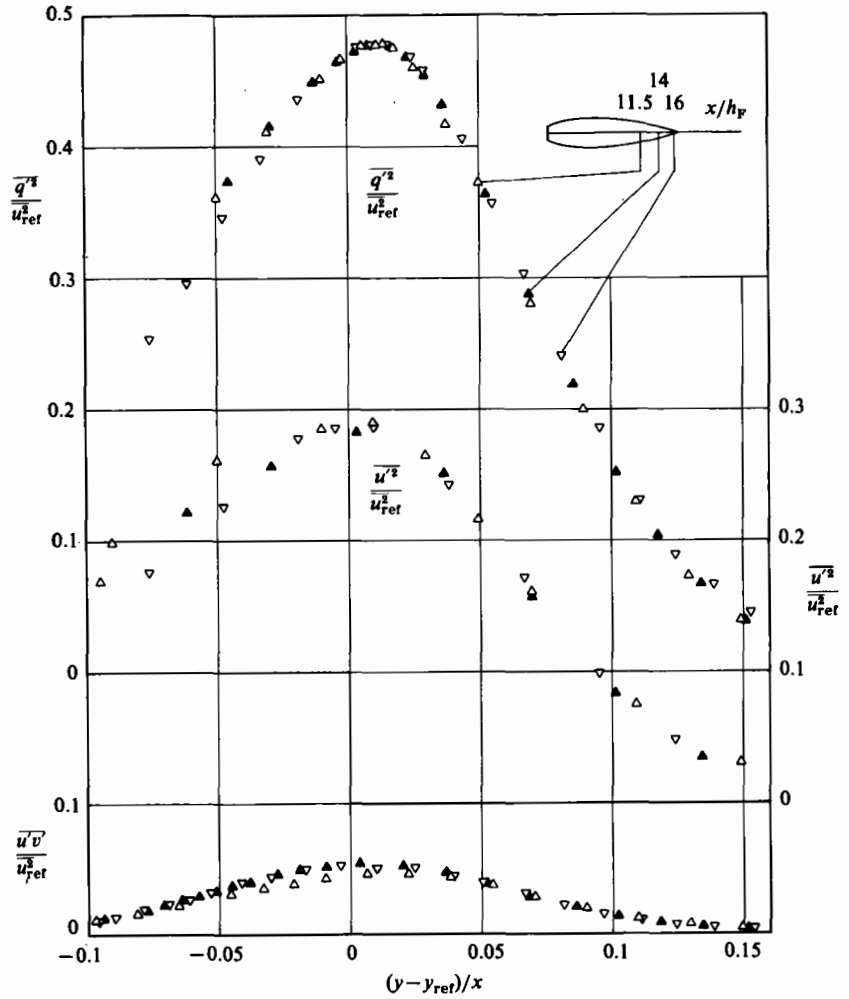

FIGURE 23. Development of fluctuating kinetic energy $\overline{q'^2}$, Reynolds normal stress $\overline{u'^2}$, and Reynolds shear stress $\overline{u'v'}$ in a curved shear layer bounding a closed reverse-flow region ($Re_{h_F} = 1.4 \times 10^4$). H.W. and P.W. data.

6.4. *Redistribution of the turbulence structure in the attached shear layer*

The redistribution of the turbulence structure in a mixing layer which encounters a wall on its high-velocity side has recently been investigated by Wood & Bradshaw (1984). Their observations are supplemented by the present investigation, where, however, the separated shear layer may have been affected differently owing to the reverse-flow region.

The peaks of the distributions of $\overline{u'v'}$ (figure 27), of $\overline{u'^2}$ (figure 28) and of $\overline{q'^2}$ (figure 29) are reduced from their values at reattachment to about half that value after a distance of only 70 % of the reattachment length x_R (full diamonds) mainly due to the presence of the wall. They also differ in the shape of the profile in the downstream direction in that the profiles $\overline{u'^2}$, $\overline{q'^2}$ and $\overline{w'^2}$ (figure 30) show a definite plateau for positions x/x_R larger than 2.28. Such a plateau does not occur in the $\overline{v'^2}$ distributions (figure 30), and this can be interpreted as a preservation of $\overline{u'^2}$ and $\overline{w'^2}$ against a decay of $\overline{v'^2}$ in the near-wall region.

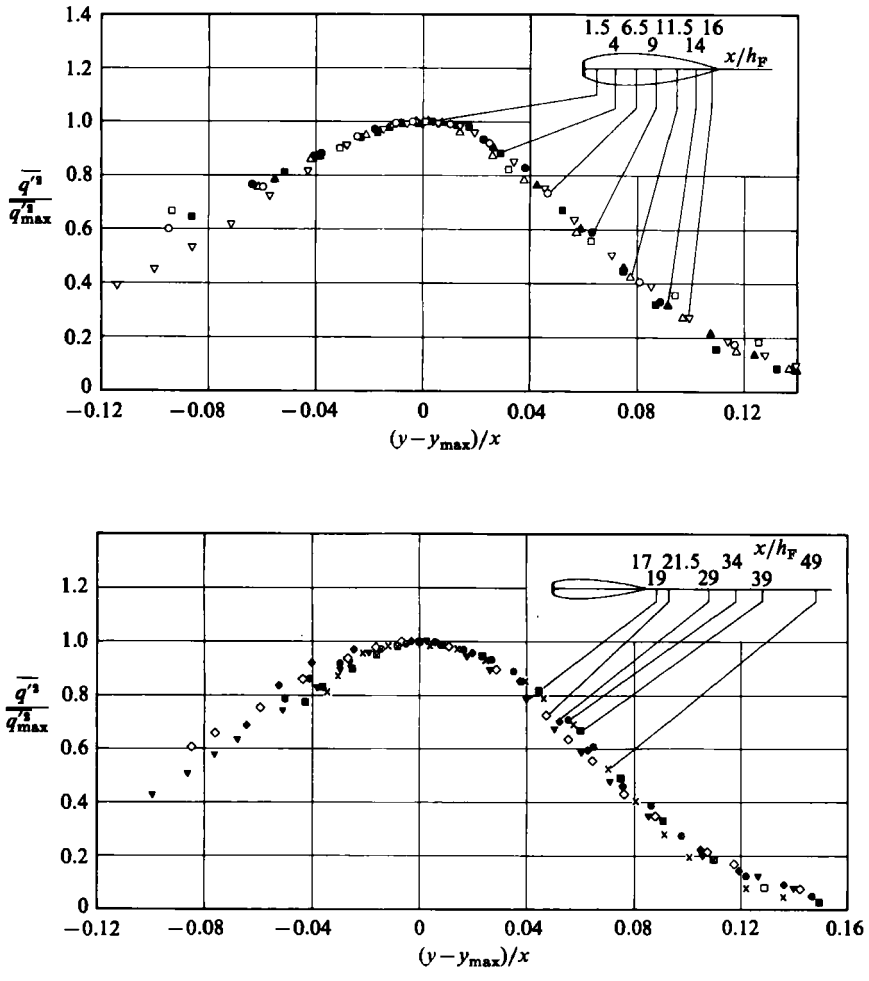

FIGURE 24. Development of fluctuating kinetic-energy profiles downstream of a bluff plate with a long splitter plate ($Re_{h_F} = 1.4 \times 10^4$). H.W. and P.W. data.

Although the hot-wire measurements of $\overline{v'^2}$, $\overline{w'^2}$ and $\overline{u'v'}$ at or close downstream of reattachment are not as reliable as the $\overline{u'^2}$ data for reasons mentioned above, their qualitative development is assumed to give the correct trend. It may therefore be concluded that the relaxation of the turbulence structure downstream of reattachment is slow, and that the profiles remain between those characteristic of a mixing layer and those of a turbulent boundary layer over a distance of at least three reattachment lengths.

A qualitative explanation for the slow return of the turbulence quantities to their distribution in a wall boundary layer may be found from an investigation by Gence & Mathieu (1980) of homogeneous turbulence. These authors have shown that the return to isotropy is slower if one component of the Reynolds normal stress (here $\overline{u'^2}$) is much larger than the two remaining ones than if two components are of about equal size and larger than the third one.

The differences in the properties of the attached shear layer and an equilibrium turbulent boundary layer may be highlighted by the following observations: (i) A

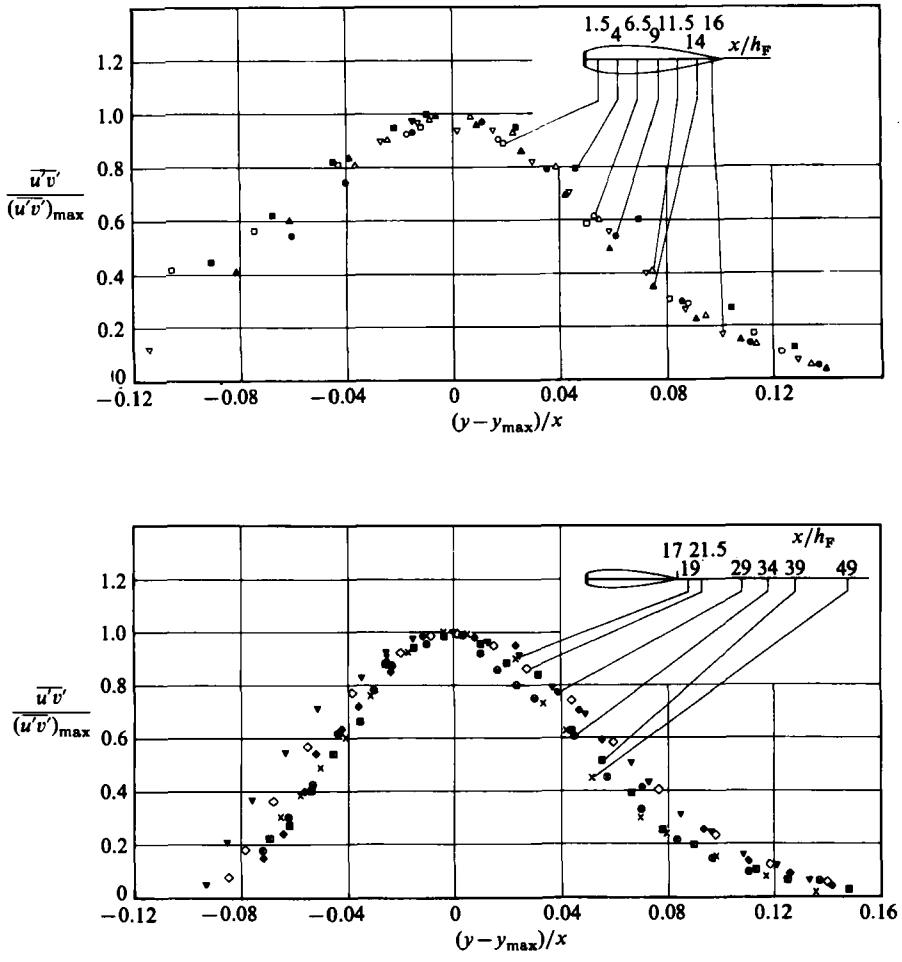

FIGURE 25. Development of Reynolds shear-stress profiles downstream of a bluff plate with a long splitter plate ($Re_{h_F} = 1.4 \times 10^4$). H.W. data.

comparison of the $\overline{u'^2}$ and $\overline{w'^2}$ distributions at $x/x_R = 2.86$ shows that they are similar in shape and magnitude, whereas $\overline{v'^2}$ is smaller by a factor of about four. This confirms Wood & Bradshaw's (1984) observations about the complex non-monotonic changes to the relative distribution of the turbulent energy among its three components. (ii) The redevelopment of the mean-velocity profile due to the wall begins with the development of the linear law in the viscous sublayer (figure 31) and continues with a slow build-up of the logarithmic law via an undershoot and then an overshoot of the mean velocity compared with the straight line of the logarithmic law. Skin friction was measured again by the wall pulsed-wire technique which, in contrast to other measuring techniques used in this region before, is independent of the effects of instantaneous reverse flow and the existence of the logarithmic law.

The undershoot in the mean-velocity profile moves further away from the wall with growing distance from reattachment and has been observed before by Bradshaw & Wong (1972). They offer two possible reasons for the departures from the logarithmic law: that the turbulence structure changes rapidly in the reattachment region; and that the lengthscale of the turbulence is not proportional to the distance

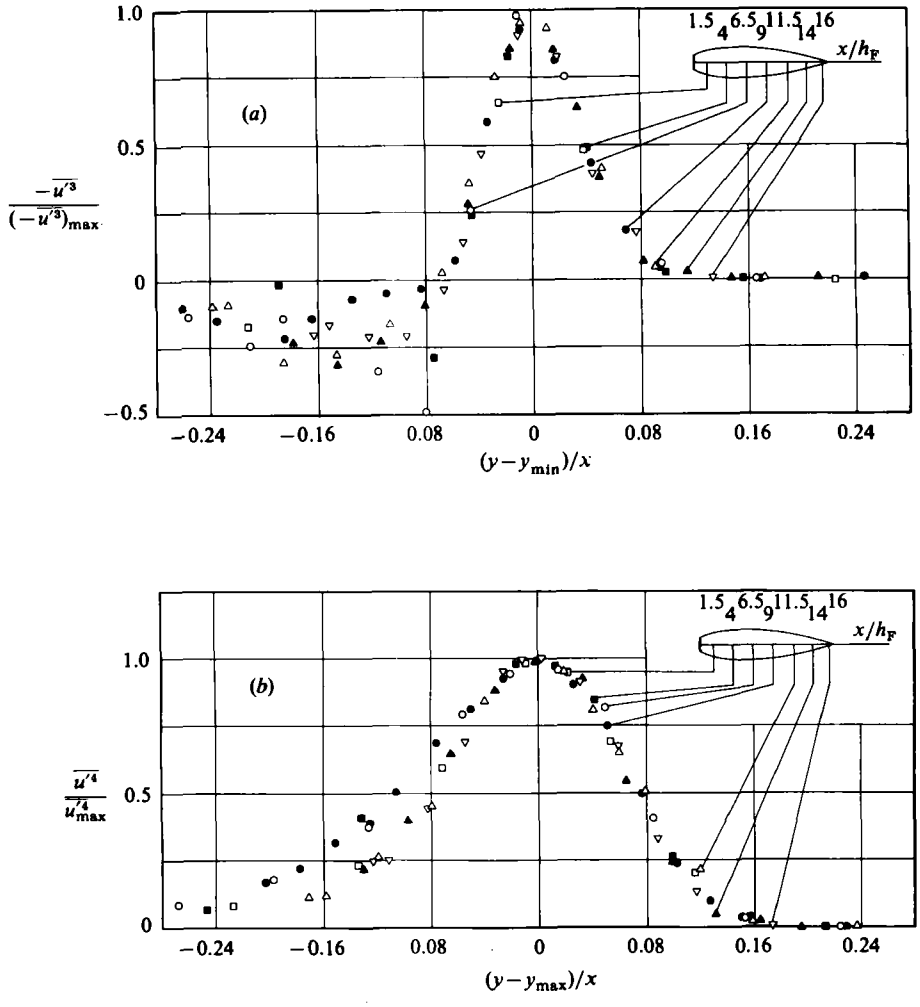

FIGURE 26. (*a*) Third-order- and (*b*) fourth-order-moment distributions in a curved shear layer bounding a closed reverse-flow region. P.W. data.

normal to the wall. Both suggestions appear to be correct, as can be seen from the redistribution of the turbulence profiles in figures 27–30 and from correlation measurements of $R_{11}^{(2)}$ and Λ_y presented in figures 32 and 33.

Figure 32 shows the distribution of the integral lengthscale Λ_y in the direction normal to the splitter plate at three positions x/x_R along the centreline. Λ_y was determined from the positive area under the distribution of the correlation coefficient $R_{11}^{(2)} = \overline{u'u'_{\Delta y}}/((\overline{u'^2}), (\overline{u'^2})_{\Delta y})^{\frac{1}{2}}$ and the open circles represent the y-position of the fixed hot-wire probe. For guidance the lines of the loci $(y/h_F)_{\overline{u'^2_{max}}}$ and $(y/h_F)_{T_{u=10\%}}$ are given.

Λ_y increases in the downstream direction but remains approximately constant in the y-direction at fixed values of x/x_R. All $R_{11}^{(2)}$ distributions used for figure 31 go through zero and then remain negative at values of about 0.05. $R_{11}^{(2)}$ distributions in

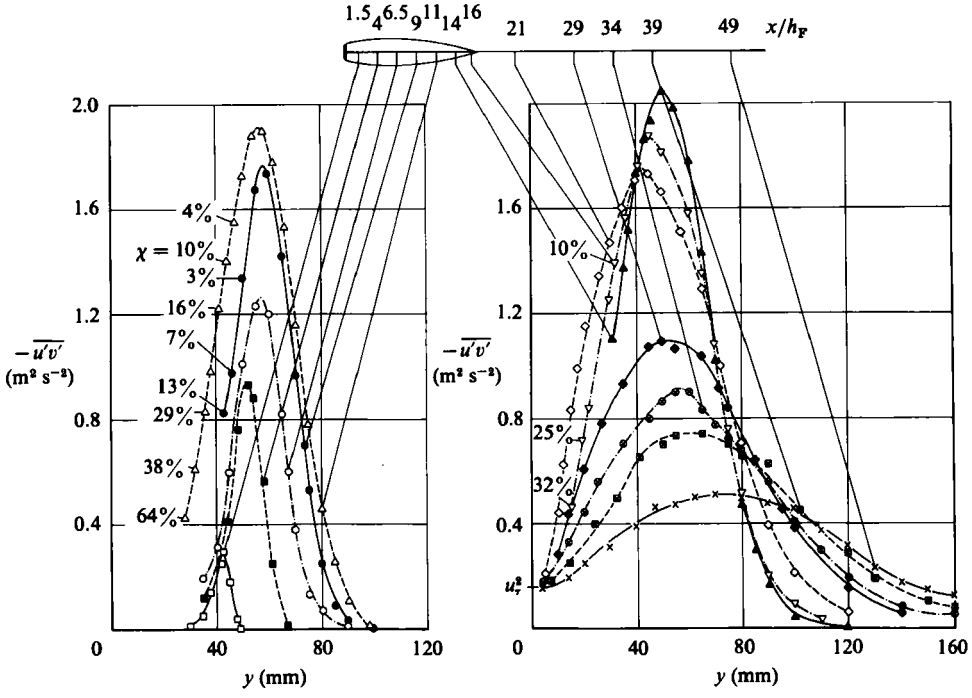

FIGURE 27. Development of the specific Reynolds shear-stress profiles downstream of a bluff plate along a splitter plate. H.W. data.

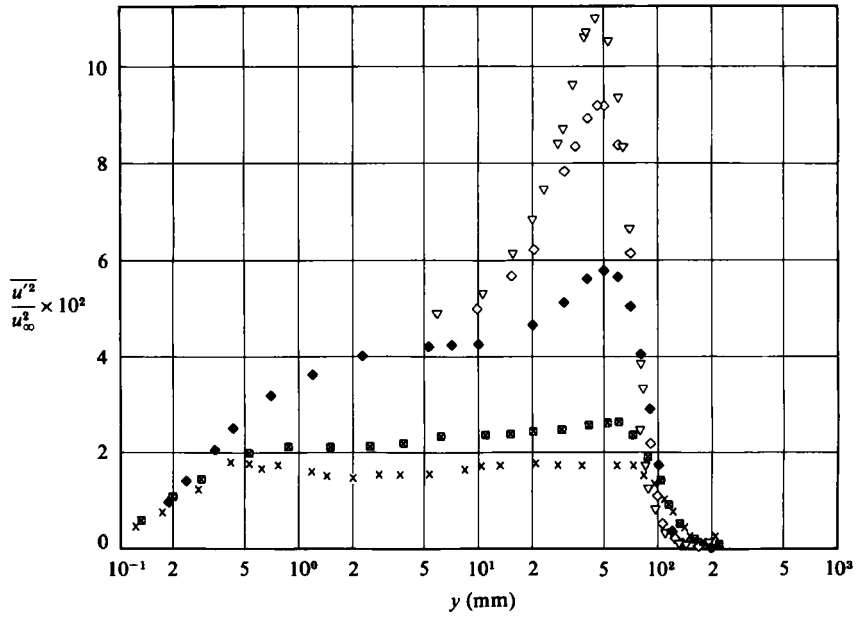

FIGURE 28. Distribution of $\overline{u'^2}$ component close to and downstream of reattachment (Re_{h_F} = 1.4 $\times 10^4$). H.W. and P.W. data: ▽, $x/x_R = 0.93$; ◇, 1.26; ◆, 1.69; ⊠, 2.28; ×, 2.86.

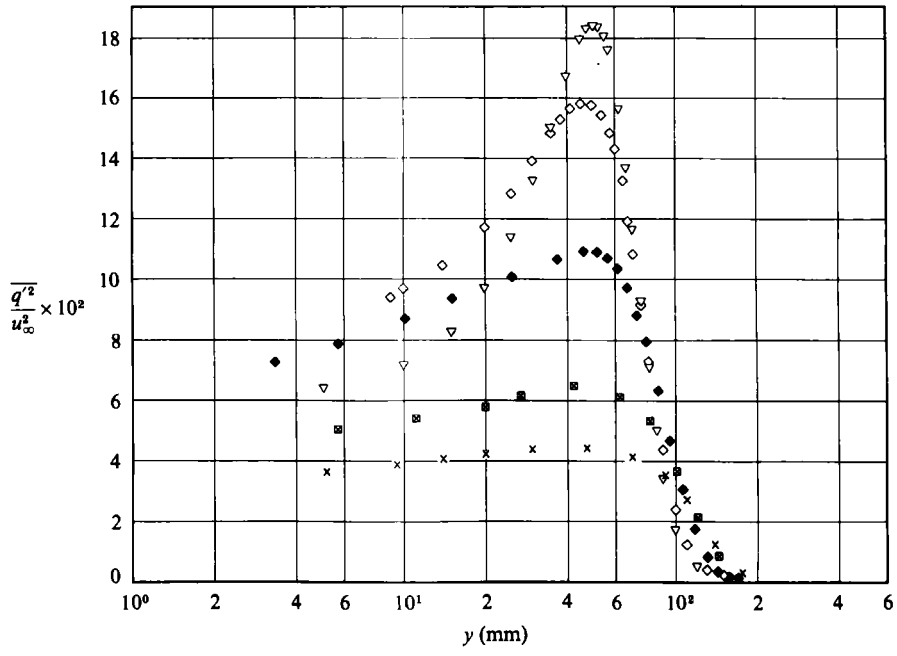

FIGURE 29. Distribution of turbulent kinetic energy close to and downstream of reattachment ($Re_{h_F} = 1.4 \times 10^4$). P.W. and H.W. data. Symbols as in figure 28.

the free stream further out in the flow than shown in figure 31 or in the empty tunnel did not tend to zero, as is to be expected. This could be due to the low intensities, to small fluctuations in the fan speed of ± 1 r.p.m. at about 1300 r.p.m. or to acoustic waves in the test section, but none of these possible effects could be shown to be the origin of this behaviour.

Knowing the distributions of the integral lengthscales Λ_z (figure 14) and Λ_y (figure 32) one can state that the large-eddy structure has lengthscales in the two cross-stream directions which are roughly equal. This confirms the three-dimensional character of the flow (e.g. figure 3) and agrees with similar results found by Pui & Gartshore (1979), for example, in plane turbulent mixing layers. In the region between the wall and approximately three fence heights h_F these lengthscales grow from about $0.5h_F$ at $x/x_R = 0.5$ to $1.5h_F$ at $x/x_R = 2.86$.

We do not claim that h_F is the adequate scaling length in the direction normal to the wall. Apart from the fence height or the locus where the mean velocity $\bar{u}$ is zero, one might use the vorticity thickness δ_ω (cf. figure 21), at least in the reverse-flow region. Further downstream $\Delta\bar{u}$ simply becomes $\bar{u}_{max}$. Λ_y/δ_ω is plotted in table 4 at three positions x/x_R and several positions y_{fp}/h_f, where y_{fp} denotes again the position of the fixed probe. The data in table 4 show that the ratio Λ_y/δ_ω varies between 0.2 and 0.3 in y- and x-directions, which is an unexpectedly small range.

6.5. *One-dimensional energy spectra*

Figure 33 presents the one-dimensional energy spectrum whose integral is $\overline{u'^2}$. Since it was not known in which regions of the complex flow investigated here the Taylor hypothesis might or might not hold, data are not given in the wavenumber presentation.

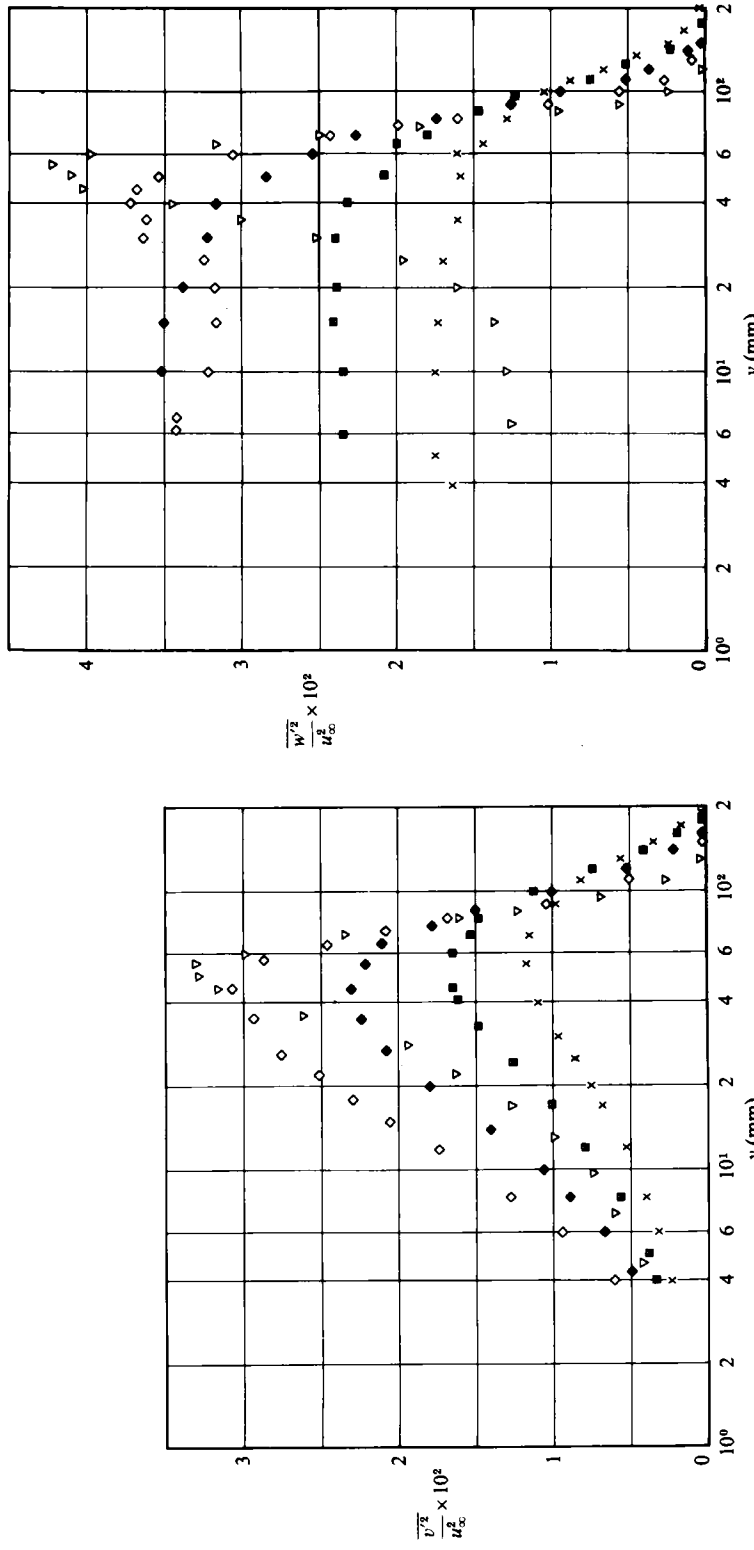

FIGURE 30. Distributions of $\overline{v'^2}$ and $\overline{w'^2}$ components close to and downstream of reattachment ($Re_{h_F} = 1.4 \times 10^4$). H.W. data. Symbols as in figure 28.

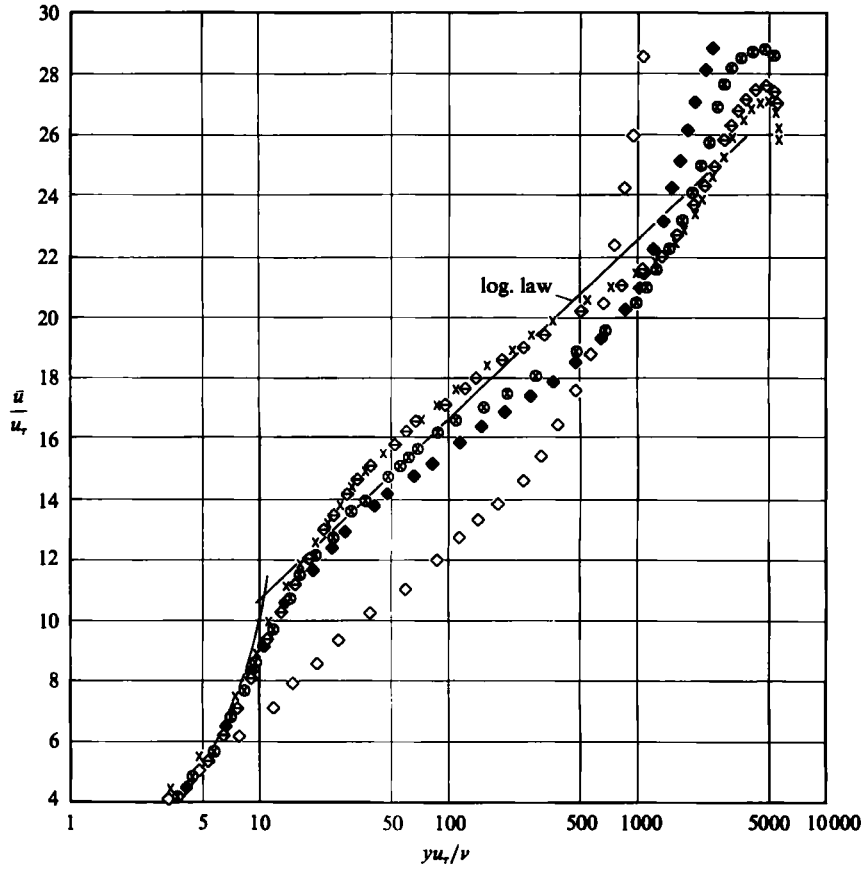

FIGURE 31. Comparison of the law of the wall with velocity profiles in a wall-bounded turbulent shear flow downstream of reattachment ($Re_{h_F} = 1.4 \times 10^4$). u_τ from wall pulsed-wire probe.

	x/h_F	x/x_R	u_τ [m/s]
◇	21.45	1.26	0.291
◆	28.95	1.69	0.374
⊗	33.95	1.99	0.387
◈	43.95	2.57	0.397
×	48.95	2.86	0.401

The spectral density Φ_{11} of $\overline{u'^2}(f)$ was measured in the frequency range $0 < f \leqslant 10000$ Hz by means of hot-wire anemometry, using a spectrum analyser (5820 A Wavetek/Rockland). Measurements were performed in the separated shear layer, in the reverse-flow region (only with $\chi > 90\,\%$) and in the reattached flow. Examples of the spectra are shown at $x/x_R = 0.38$, 1.26 and 2.86 at two or three positions y normal to the splitter plate (cf. caption of figure 33). The spectral density was made dimensionless by the local mean velocity $\bar{u}$ and the distance x from separation, instead of by u_∞ and $x - x_0$ as in Wood & Bradshaw (1982), and is defined as

$$\Phi'_{11} = \frac{|\bar{u}|}{x} \Phi_{11}(f). \tag{6.2}$$

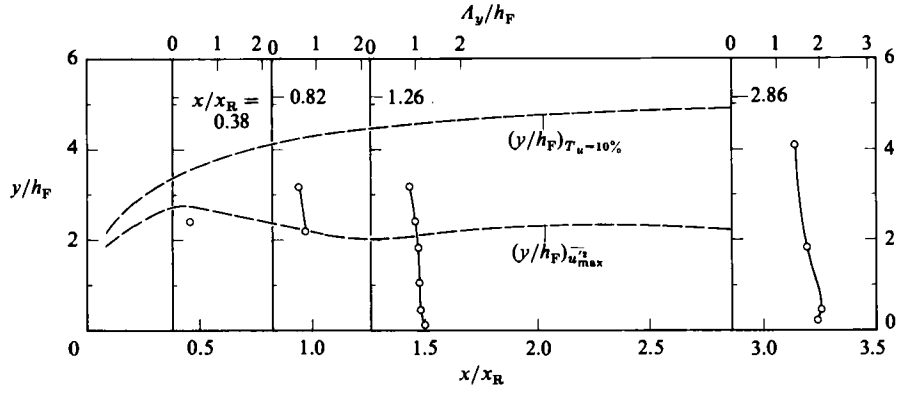

FIGURE 32. Distributions of the integral lengthscale Λ_y in the normal direction to the splitter plate at four positions x/x_R along the centreline ($Re_{h_F} = 1.4 \times 10^4$).

x/x_R	0.38	0.82					1.26			
y_{tp}/h_F	2.41	2.18	3.18	0.11	0.20	0.46	1.05	1.82	2.41	3.18
Λ_y/δ_ω	0.273	0.278	0.218	0.227	0.220	0.210	0.206	0.201	0.187	0.161

TABLE 4

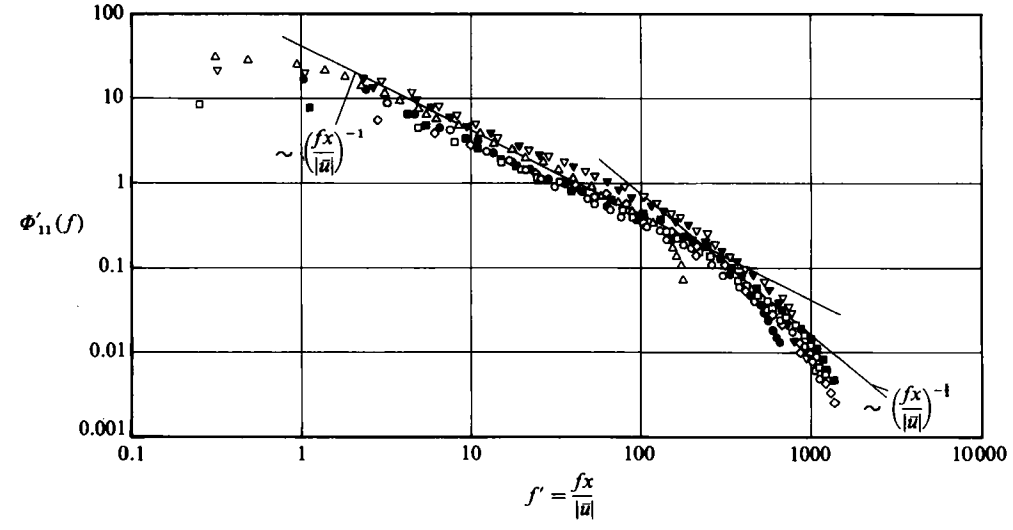

FIGURE 33. One-dimensional energy spectra along the centreline at three stations x/x_R and at several positions normal to the splitter plate ($Re_{h_F} = 1.4 \times 10^4$).

$x/x_R = 0.38$	$= 1.26$	$= 2.86$
◇ $y = 1$ mm	▽ = 10 mm	■ = 10 mm
▲ $y = 55$ mm	▼ = 40 mm	□ = 40 mm
	● = 80 mm	○ = 80 mm

ϕ'_{11} is plotted against the non-dimensional frequency f', where

$$f' = \frac{fx}{|\bar{u}|} \tag{6.3}$$

and

$$\Phi_{11} = \frac{\overline{(u'^2(f))}/\Delta f}{\overline{(u'^2)}_{\text{tot}}}, \tag{6.4}$$

with $\overline{(u'^2(f)}/\Delta f)$ as the energy share per filter bandwidth Δf ($\Delta f = 25$ Hz) at the frequency f and $\overline{u'^2_{\text{tot}}}$ as the turbulence energy summed up over the whole frequency range. Plotting Φ'_{11} against f' leads to a transformation of the ordinate and the abscissa values.

As may be seen from figure 33 the Φ'_{11} distributions show no spectral peak. They are proportional to $(f')^{-1}$ in the frequency range of about $1 < f' < 250$ (cf. Hinze, p. 354) and to $(f')^{-\frac{5}{3}}$ in the range $250 < f' < 700$. What is even more astonishing is the fact that they behave almost similarly over the whole frequency range irrespective of the part of the flow they were measured in.

It may finally be noted that periodic vortex shedding, which was observed at a smaller Reynolds number ($Re_{h_F} = 1.5 \times 10^3$) in the separated shear layer very close to separation, could not be detected at the higher Reynolds number 1.4×10^4.

7. Conclusions

It has been shown that in the present experiment the flow downstream of a bluff plate with a long splitter plate is affected by strong three-dimensional effects off the centreline. These effects are manifested by the curved reattachment line and by other flow measurements. The large-eddy structure in the inner region ($y \lesssim 3h_F$) had lengthscales in the two cross-stream directions which were approximately equal, in agreement with the results of Pui & Gartshore (1979) and others. Integral lengthscales, Λ_y and Λ_z, increase in downstream direction, indicating a growth of the turbulence structure, but no return to a two-dimensional structure as observed just downstream from separation at the bluff plate could be found.

The separated shear layer on the centreline has only a small self-preserving region upstream of reattachment, but both the separated and the reattached shear flows show large regions where individual profile families, such as $\overline{u'v'}$ and $\overline{q'^2}$, are similar (profile similarity).

Mean velocity and r.m.s. fluctuations in the reverse-flow region reach values of up to $0.3\bar{u}_{\max}$ and $0.5\,(\overline{u'^2_{\max}})^{\frac{1}{2}}$ respectively, whereas the mean skin friction is of the same order of magnitude in the reverse-flow region and in the reattached flow.

Neither in the reverse-flow region nor half a bubble length downstream of reattachment does the near-wall flow follow the logarithmic law of the wall. This has consequences for some calculation methods and some measuring techniques for the skin friction.

Owing to the relatively short length of the splitter plate (about $68h_F$) the development of the attached flow into an equilibrium boundary layer could not be observed.

The dimensionless spectral-density distributions show no peak and are similar over the whole frequency range irrespective of the part of the flow they were measured in.

The authors, especially R. Ruderich, thank the Deutsche Forschungsgemeinschaft for the financial support of this investigation and appreciate the discussions with their colleagues at Imperial College London, at the University of Surrey and at the Hermann-Föttinger-Institut.

REFERENCES

ARIE, M. & ROUSE, H. 1956 Experiments on two-dimensional flow over a normal wall. *J. Fluid Mech.* **1**, 129–141.

BRADBURY, L. J. S. & CASTRO, I. P. 1971 A pulsed-wire technique for velocity measurements in highly turbulent flows. *J. Fluid Mech.* **49**, 657–691.

BRADSHAW, P. & WONG, F. Y. F. 1972 The reattachment and relaxation of a turbulent shear layer. *J. Fluid Mech.* **52**, 113–135.

BROWN, G. L. & ROSHKO, A. 1974 On density effects and large structure in turbulent mixing layers. *J. Fluid Mech.* **64**, 775–816.

CASTRO, I. P. & DIANAT, M. 1983 Surface flow patterns on rectangular bodies in thick boundary layers. *J. Wind Engng Indust. Aerodyn.* **11**, 107–119.

CHANDRASUDA, C. & BRADSHAW, P. 1981 Turbulence structure of a reattaching mixing layer. *J. Fluid Mech.* **110**, 171–194.

CHERRY, N. J., HILLIER, R. & LATOUR, M. E. M. P. 1984 Unsteady measurements in a separated and reattaching flow. *J. Fluid Mech.* **144**, 13–46.

DAHM, A. & VAGT, J. D. 1977 Entwicklung und Herstellung interferenzarmer Hitzdrahtsonden. *HFI Inst.* 01/77.

DE BREDERODE, V. & BRADSHAW, P. 1972 Three-dimensional flow in nominally two-dimensional separation bubbles. I. Flow behind a rearward-facing step. *Imperial College Aero Rep.* 72-19.

DE BREDERODE, V. A. S. L. 1975 Three-dimensional effects in nominally two-dimensional flow. Ph.D. thesis, Imperial College, London University.

DENGEL, P., FERNHOLZ, H. H. & VAGT, J.-D. 1982 Turbulent and mean flow measurements in an incompressible axisymmetric boundary layer with incipient separation. *Turbulent Shear Flows 3* (ed. Bradbury *et al.*). Springer.

EATON, J. K. & JOHNSTON, J. P. 1980 Turbulent flow reattachment. An experimental study of the flow and structure behind a backward-facing step. *Rep. MD*-39. Stanford University.

EATON, J. K. & JOHNSTON, J. P. 1981 A review of research on subsonic turbulent flow reattachment. *AIAA J.* **19**, 1093–1100.

FERNHOLZ, H. H., GRAHAM, J. M. R. & VAGT, J.-D. 1982 A wind tunnel for unsteady turbulent shear flows: design and flow calculation. *Z. Flugwiss. Weltraumforschung* **6**, 408–416.

FERNHOLZ, H. H. & VAGT, J.-D. 1981 Turbulence measurements in an adverse-pressure-gradient three-dimensional turbulent boundary layer along a circular cylinder. *J. Fluid Mech.* **111**, 233–269.

FROEBEL, E. & VAGT, J.-D. 1974 Ein automatisch abgleichendes Flüssigkeitsmanometer mit digitaler Anzeige. *DLR-FB* 74-40.

GENCE, J. N. & MATHIEU, J. 1980 The return to isotropy of homogeneous turbulence having been submitted to two successive plane strains. *J. Fluid Mech.* **101**, 555–566.

GINDER, R. B. & BRADBURY, L. J. S. 1973 Preliminary investigation of a pulsed-gauge technique for skin friction measurements in highly turbulent flow. ARC Paper 34448.

HILLIER, R. 1978 Further measurements in a separated and reattaching flow. Imperial College London, Dept of Aeronautics.

HILLIER, R. & CHERRY, N. J. 1981 The effects of stream turbulence on separation bubbles. *J. Wind Engng Indust. Aero.* **8**, 49–58.

HILLIER, R., LATOUR, M. E. M. P. & CHERRY, N. J. 1983 Unsteady measurements in separated- and reattaching flows. *4th Turbulent Shear Flow Conf. Karlsruhe.*

KIYA, M., SASAKI, K. & ARIE, M. 1982 Discrete vortex simulation of a turbulent separation bubble. *J. Fluid Mech.* **120**, 219–244.

KIYA, M. & SASAKI, K. 1983 Structure of a turbulent separation bubble. *J. Fluid Mech.* **137**, 83–113.

KOTTKE, V. 1983 Strömung, Stoff-, Wärme- und Impulsübertragung in lokalen Ablösegebieten. *Fortschrittsberichte VDI-Z.* Reihe 7 Nr. 77.

KREPLIN, H. P. 1976 Experimentelle Untersuchungen der Längsschwankungen und der wandparallelen Querschwankungen der Geschwindigkeit in einer turbulenten Kanalströmung. DFVLR-Verlag u. MPI-Göttingen.

MENSING, P. & FIEDLER, H. 1980 Eine Methode zur Sichtbarmachung von hochturbulenten Luftströmungen mit grossen Reynolds-Zahlen. *Z. Flugwiss. Weltraumforschung* **4**, 366–368.

PATEL, V. C. 1965 Calibration of the Preston tube and limitations on its use in pressure gradients. *J. Fluid Mech.* **23**, 185–208.

PUI, N. K. & GARTSHORE, I. S. 1979 Measurements of the growth rate and structure in plane turbulent mixing layers. *J. Fluid Mech.* **91**, 111–130.

RANGA RAJU, K. G. & GARDE, R. J. 1970 Resistance of an inclined plate placed on a plane boundary in two-dimensional flow. *Trans. ASME* D: *J. Basic Engng* **92**, 21–31.

ROGERS, B. K. & HEAD, M. R. 1969 Measurements of three-dimensional boundary layers. *J. R. Aeronaut. Soc.* **73**, 796–798.

ROSHKO, A. & LAU, J. C. 1965 Some observations on transition and reattachment of a free shear layer in incompressible flow. In *Proc. 1965 Heat Transfer and Fluid Mech. Inst.*

RUDERICH, R. & FERNHOLZ, H. H. 1983 An experimental investigation of the turbulent shear flow downstream of a normal flat plate with a long splitter plate-modification of a model. *4th Turbulent Shear Flow Conf., Karlsruhe.*

SIMPSON, R. L. 1976 Interpreting laser and hot-film anemometer signals in a separating boundary layer. *AIAA J.* **14**, 124–126.

SMITS, A. J. 1980 A visual study of a separation bubble. In *Intl Symp. on Flow Visualization, Bochum.*

SMITS, A. J. 1982 Scaling parameters for a time-averaged separation bubble. *Trans. ASME* I: *J. Fluids Engng* **104**, 178–184.

STEVENSON, W. H., THOMPSON, H. D. & CRAIG, R. R. 1984 Laser velocimeter measurements in highly turbulent recirculating flows. *Trans. ASME* I: *J. Fluids Engng* **106**, 173–180.

TUTU, N. K. & CHEVRAY, R. 1975 Cross-wire anemometry in high turbulence. *J. Fluid Mech.* **71**, 785–800.

VAGT, J.-D. 1979 Hot-wire probes in low speed flow. *Prog. Aero. Sci.* **18**, 271–325.

WESTPHAL, R. V., JOHNSTON, J. P. & EATON, J. K. 1984 Experimental study of flow reattachment in a single-sided sudden expansion. *NASA Contractor Rep.* 3765.

WOOD, D. & BRADSHAW, P. 1983 A turbulent mixing layer constrained by a solid surface. Part 1. Measurements before reaching the surface. *J. Fluid Mech.* **122**, 57–89.

WOOD, D. & BRADSHAW, P. 1984 A turbulent mixing layer constrained by a solid surface. Part 2. Measurements in the wall-bounded flow. *J. Fluid Mech.* **139**, 347–361.

WYGNANSKI, I. & FIEDLER, H. E. 1970 The two-dimensional mixing region. *J. Fluid Mech.* **41**, 327–361.